AD-A104 554 SRI INTERNATIONAL MENLO PARK CA F/G 4/1
ALTAIR RADAR STUDY OF EQUATORIAL SPREAD F.(U)
FEB 81 R T TSUNODA DNA001-79-C-0153
UNCLASSIFIED DNA-5689F NL

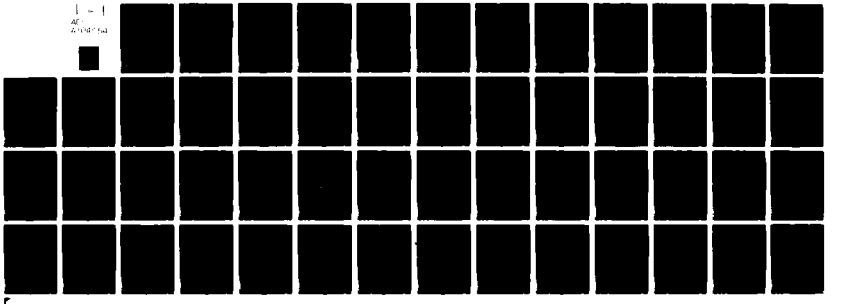

END
DATE FILMED
'0 8!
DTIC

LEVEL II

12

DNA 5689F

ALTAIR RADAR STUDY OF EQUATORIAL SPREAD F

Roland T. Tsunoda
SRI International
333 Ravenswood Avenue
Menlo Park, California 94025

1 February 1981

Final Report for Period 11 January 1979—30 November 1980

CONTRACT No. DNA 001-79-C-0153

APPROVED FOR PUBLIC RELEASE;
DISTRIBUTION UNLIMITED.

THIS WORK SPONSORED BY THE DEFENSE NUCLEAR AGENCY
UNDER RDT&E RMSS CODE B322079462 I25AAXHX64009 H2590D.

Prepared for
Director
DEFENSE NUCLEAR AGENCY
Washington, D. C. 20305

Destroy this report when it is no longer needed. Do not return to sender.

PLEASE NOTIFY THE DEFENSE NUCLEAR AGENCY, ATTN: STTI, WASHINGTON, D.C. 20305, IF YOUR ADDRESS IS INCORRECT, IF YOU WISH TO BE DELETED FROM THE DISTRIBUTION LIST, OR IF THE ADDRESSEE IS NO LONGER EMPLOYED BY YOUR ORGANIZATION.

UNCLASSIFIED

SECURITY CLASSIFICATION OF THIS PAGE (When Data Entered)

REPORT DOCUMENTATION PAGE

READ INSTRUCTIONS BEFORE COMPLETING FORM

1. REPORT NUMBER: DNA 5689F	2. GOVT ACCESSION NO.: AD-A104 554
3. RECIPIENT'S CATALOG NUMBER:	
4. TITLE (and Subtitle): ALTAIR RADAR STUDY OF EQUATORIAL SPREAD F.	5. TYPE OF REPORT & PERIOD COVERED: Final Report, ~~for Period~~ 11 Jan 79-30 Nov 80
	6. PERFORMING ORG. REPORT NUMBER: SRI Project 8164
7. AUTHOR(s): Roland T. Tsunoda	8. CONTRACT OR GRANT NUMBER(s): DNA 001-79-C-0153
9. PERFORMING ORGANIZATION NAME AND ADDRESS: SRI International, 333 Ravenswood Avenue, Menlo Park, California 94025	10. PROGRAM ELEMENT, PROJECT, TASK AREA & WORK UNIT NUMBERS: Subtask I25AAXHX640-09
11. CONTROLLING OFFICE NAME AND ADDRESS: Director, Defense Nuclear Agency, Washington, D.C. 20305	12. REPORT DATE: 1 February 1981
	13. NUMBER OF PAGES: 54
14. MONITORING AGENCY NAME & ADDRESS (if different from Controlling Office): 12 X640 13 54	15. SECURITY CLASS (of this report): UNCLASSIFIED
	15a. DECLASSIFICATION/DOWNGRADING SCHEDULE:

16. DISTRIBUTION STATEMENT (of this Report)

Approved for public release; distribution unlimited.

17. DISTRIBUTION STATEMENT (of the abstract entered in Block 20, if different from Report)

18. SUPPLEMENTARY NOTES

This work sponsored by the Defense Nuclear Agency under RDT&E RMSS Code B322079462 I25AAXHX64009 H2590D.

19. KEY WORDS (Continue on reverse side if necessary and identify by block number)

Equatorial spread F
Ionospheric irregularities
Plasma bubbles
Backscatter plumes

20. ABSTRACT (Continue on reverse side if necessary and identify by block number)

The results of research on equatorial spread-F (ESF) phenomena obtained by using two backscatter radars, ALTAIR and TRADEX, are summarized. The radar measurements were made in support of three rocket campaigns conducted from the Kwajalein Atoll during the summers of 1977 through 1979. Backscatter data from ESF irregularities and incoherent-scatter (IS) data from thermal plasma fluctuations were used to show that the structuring of the equatorial F-region plasma is initiated by large-scale (tens to a few hundred

DD FORM 1 JAN 73 1473 EDITION OF 1 NOV 65 IS OBSOLETE

UNCLASSIFIED

SECURITY CLASSIFICATION OF THIS PAGE (When Data Entered)

410 21

20. ABSTRACT (Continued)

kilometers in the east-west direction) plasma-density modulations in the bottomside F layer. The modulation, best described by wavelike altitude variations in constant electron-density contours, appears to be imposed on the bottomside F layer around E-region sunset by a yet-to-be-identified source (although atmospheric gravity waves are a likely candidate). The amplification of the wavelike modulation, in the form of upwellings from the crests of the modulation, is consistent with the amplification expected from the collisional Rayleigh-Taylor instability. Once the upwellings begin to grow in altitude extent, the west walls become unstable via the gradient-drift instability, driven by an eastward neutral wind blowing through the walls of the upwellings. The enhanced structuring of the west wall at low F-region altitudes is made possible by the presence of a velocity shear in eastward plasma drift. That is, the velocity shear results in a larger relative ("slip") velocity between the plasma and neutral gas, a factor that directly determines the growth rate of the gradient-drift instability. Because the slip velocity is much larger than the equivalent gravity-driven velocity that determines the growth rate of the collisional Rayleigh-Taylor instability, structuring at low altitudes is dominated by the gradient-drift instability. In fact, the west wall of an upwelling in the bottomside F layer can be likened to a large barium ion cloud, which also structures via the wind-driven gradient-drift instability. At high altitudes, however, structuring in plasma "bubbles" that develop upward from crests of upwellings is produced primarily by the collisional Rayleigh-Taylor instability. Smaller-scale irregularities such as those that produce radar backscatter are believed to be generated by drift waves that grow from steep gradients associated with the walls of upwellings and plasma bubbles, or with larger-scale irregularities.

TABLE OF CONTENTS

LIST OF ILLUSTRATIONS

LIST OF TABLES

I INTRODUCTION

Equatorial spread-F (ESF) phenomena have received considerable attention in recent years from both the defense and scientific communities. The impetus for this interest in equatorial irregularities was the surprising discovery that radio waves with frequencies in the gigahertz range can scintillate significantly after traversal through a disturbed equatorial ionosphere (Crampton and Sessions, 1971; Christiansen, 1971; Craft and Westerlund, 1972). Because the current trend is to move satellite communication channels upward in frequency from the lower UHF band to the gigahertz range (where ionospheric effects were thought to be innocuous), this discovery required serious reassessment of ionospheric irregularity characteristics and their source mechanisms. Understanding of the natural processes that produce the intense irregularities is also requisite for extrapolation of these effects to communication systems operating in a nuclear environment.

Extrapolation of systems effects produced by equatorial irregularities to the nuclear case is of particular interest to the Defense Nuclear Agency (DNA) because the source mechanism that initiates ESF structure is believed to be a direct analog of the gradient-drift instability, the dominant source of scintillation-producing structure in a nuclear environment (e.g., Workman, 1977). Therefore, the attraction of ESF phenomena from DNA's point of view is its direct relevance for predicting systems effects in a nuclear environment and for understanding nuclear phenomenology.

In Summer 1977, DNA sponsored a rocket campaign conducted from the Kwajalein Atoll, Marshall Islands, to investigate ESF phenomena. The objective was to coordinate rocket in-situ measurements of ESF structure with scintillation measurements using the DNA Wideband satellite (e.g., Rino et al., 1980). ALTAIR, a backscatter radar located in the Kwajalein Atoll, was utilized in that program as a monitor of ESF activity. ALTAIR

was repeatedly scanned in the magnetic east-west direction to detect and track regions of strong ESF backscatter into the rocket launch corridor. The intent was to try to occult one of these strong, altitude-extended backscatter regions (called "plumes") with the Wideband satellite while launching a rocket through the most disturbed region. A similar program was attempted in 1978.

SRI International (SRI) provided backup support to the ALTAIR project (Dr. D. M. Towle, MIT Lincoln Laboratory) during the 1977 and 1978 field programs through its involvement with the Wideband satellite project. While acting in that capacity, we demonstrated (using 1977 ALTAIR data) that incoherent-scatter (IS) returns were contained in ALTAIR backscatter measurements and that electron-density profiles were readily computed from the recorded data (Tsunoda et al., 1978, 1979).[1,2*] With DNA's approval, we conducted a set of experiments in 1978 (adjunct to the rocket program) that were specifically designed to exploit the IS capability of ALTAIR. The experiment was designed to measure the background F-layer characteristics that were associated with the presence of ESF structure.

In 1979, a third DNA rocket campaign was conducted from the Kwajalein Atoll. In this program the objective was modified from that in 1977 and 1978 so that strong ESF structure characteristics could be measured in-situ by rockets, supported by ground-based experiments, without requiring coordinated measurements with the Wideband satellite. The rockets were decoupled from Wideband satellite passes in order to increase the number of opportunities for a rocket launch into strong ESF activity. With the decoupling of the rocket program from Wideband satellite passes, the principal responsibility for detecting ESF activity fell on ALTAIR. (SRI assumed ALTAIR project responsibility for this field program.) The objectives were (1) to predict in real time the time of arrival of strong backscatter plumes in the rocket launch corridor, and (2) to establish a data base of ESF backscatter measurements and corresponding IS measurements of the background F layer.

---

*Superscripts correspond to numbered references listed in the Appendix.

A major practical problem concerning rocket launch criteria based on ALTAIR measurements (instead of scintillation measurements with the Wideband satellite) was the spatial relationship of the intense, scintillation-producing irregularities to the meter-scale, backscatter-producing irregularities. Radar measurements had already indicated that ESF backscatter plumes were highly localized in east-west extent (e.g., Woodman and LaHoz, 1976; Tsunoda et al., 1978,[1] 1979;[2] Towle, 1980). If they were collocated, ALTAIR spatial maps of backscatter distribution could be used to locate strong scintillation-producing irregularity regions into which the rockets could be launched. On the other hand, if they were not spatially collocated, ALTAIR maps would be no more useful than a general ESF activity monitor.

In preparation for the 1979 Kwajalein rocket campaign, analyses of 1977 and 1978 ALTAIR data were conducted (1) to determine the spatial relationship of larger-scale ESF structure to radar backscatter, and (2) to characterize the temporal evolution of ESF plumes. The results were used as the basis for the 1979 rocket launch criteria.

In addition to ALTAIR, a second radar--TRADEX--was also operated in support of the 1979 rocket program. The objective of this radar experiment was to characterize the small-scale end of the spectrum of ESF irregularities. Until ALTAIR measurements of 1-m and 36-cm ESF irregularities were made, the small-scale end of the ESF spectrum was believed to terminate around 6 m, the ion gyroradius in the equatorial F layer (Woodman and Basu, 1978). Backscatter observations at 1320 MHz with TRADEX were intended to extend the detected spectrum of irregularity scale sizes down to 11 cm.

In this final report, we summarize the results derived from the analyses of ALTAIR and TRADEX data obtained during the three Kwajalein rocket campaigns. Details of these results have already been published as DNA topical reports, which are listed in the Appendix. Results of the most recent data analysis (concerning the role of velocity shear in plasma flow on ESF generation), which have not appeared as a topical report, are discussed in detail in Section III-E.

The remainder of the report is divided into three sections. In Section II, we describe the ALTAIR and TRADEX radars, the operational modes used, and the data collected during the three rocket campaigns. The results are summarized in chronological order in Section III, and are discussed in Section IV. The discussion consists of an interpretation of the results obtained thus far in terms of a descriptive model of ESF structure development. A key conclusion is that ESF phenomena represent a versatile means of investigating certain nuclear phenomenology questions.

II EXPERIMENTAL CONSIDERATIONS

A. Description of the ALTAIR and TRADEX Radars

The Kwajalein radar complex includes the ALTAIR (ARPA Long-Range Tracking And Instrumentation Radar) and TRADEX (Target Resolution And Discrimination Experiments) radars; both are located on Roi-Namur Island in the Kwajalein Atoll, Marshall Islands (9.4°N, 167.5°E, geographic coordinates). Both radars are part of a U.S. Army sponsored research program to study the physical interaction between a vehicle in ballistic flight and its natural environment, with particular emphasis on reentry. The radars, however, have also been utilized in the DNA-sponsored field experiments on equatorial spread-F studies because of their unique capabilities and favorable geographic location. (The magnetic dip latitude of the Kwajalein radar complex is 4.3°N, well within the zone characterized by equatorial spread-F phenomena.)

ALTAIR is a highly sensitive, dual-frequency radar that operates simultaneously at 155.5 MHz (VHF) and 415 MHz (UHF). The radar utilizes a fully steerable 45.7-m (150-ft) paraboloid antenna. Its full steerability has been shown to be extremely useful in the investigation of equatorial spread-F phenomena (see Section III). ALTAIR has been shown to be sensitive enough for incoherent-scatter measurements at both frequencies (Tsunoda et al., 1978,[1] 1979;[2] Towle, 1980). Other pertinent ALTAIR radar characteristics are listed in Table 1. Further details of ALTAIR are given in Tsunoda et al. (1978, 1979)[1,2] and Towle (1980).

ALTAIR has a variety of waveforms that could be used; however, the pulsewidths listed in Table 1 are those most commonly used for both incoherent-scatter and semicoherent scatter measurements. The more recently developed waveforms that are useful for ionospheric studies include a 238-μs pulsewidth at VHF, and double-pulse (or pulse-pair) waveforms at both VHF and UHF. These waveforms were utilized for the first time in ionospheric backscatter experiments during the 1980 experiments.

Table 1

RADAR SYSTEM CHARACTERISTICS

Characteristics	ALTAIR		TRADEX
	VHF	UHF	
Frequency, MHz	155.5	415	1320
Peak power, MW	10	20	4
Pulsewidth, μs	30	40	40/1.7 (chirp)
Antenna			
Diameter, m (ft)	45.7 (150)	45.7 (150)	25.6 (84)
Beamwidth, deg	2.8	1.1	0.65
Gain, dB	34.7	42.4	48.5
Effective aperture, m^2	820	722	283
Temperature, K	992	785	622
Polarization	LC/RC	LC/RC	LC/RC

Other available waveforms have much shorter pulsewidths than those listed, and are intended primarily for satellite track-and-identification studies. Waveforms with 37-m range resolution have been employed, however, for a limited amount of equatorial spread-F backscatter measurements (Huba *et al.*, 1978) as well as for total electron content measurements by using the differential group delay between VHF and UHF to satellites of opportunity (Tsunoda and Towle, 1979).[3,4] Amplitude scintillation measurements have also been made using these short waveforms, again by skin-tracking satellites of opportunity.

The standard mode of ALTAIR operation was an east-west scan made with the radar beam directed perpendicularly with the geomagnetic field at F-region altitudes. (The scan plane can be visualized as being oriented approximately in the geomagnetic east-west direction, where Magnetic North is at 8.5°E true azimuth, and tilted about 9° north of vertical.) This field-perpendicular scan was used to map the spatial distribution of ESF backscatter regions. Maps of this kind, taken sequentially, could then be used to determine the dynamics and time evolution of these backscatter regions.

In 1977, the field-perpendicular scan consisted of 21 discrete positions covering an angular sector of 45°, and taking about 6 minutes to complete the scan. In 1978, the scan was expanded to 25 steps covering a 72° angular sector with a scan time of about 8 minutes. In 1979 and 1980, the field-perpendicular scan was modified into a continuous scan with variable angular sector coverage and scan rates. The maximum sector coverage was 120°.

Other ALTAIR scan modes included latitude scans (or elevation scans in the magnetic meridian) and off-perpendicular scans. Both of these scans were implemented in 1978 for incoherent-scatter measurements of the background F-region plasma. In 1978, both scan modes were executed manually, in discrete steps with selected dwell times at each position. In 1979 and 1980, continuous scans were implemented for these modes. These scans were particularly useful in detecting and characterizing plasma bubbles.

TRADEX is also a highly sensitive, dual-frequency radar. It operates simultaneously at 1320 MHz (L band) and 2350.8 MHz (S band); however, only the L-band channel is useful for incoherent-scatter and ionospheric backscatter measurements. This radar is located within a few hundred meters of ALTAIR and utilizes a fully steerable 25.6-m (84-ft) paraboloid antenna. Other pertinent TRADEX parameters are listed in Table 1. Thus far, TRADEX has been used only to detect backscatter from equatorial field-aligned irregularities (Tsunoda, 1980).[8] In its present configuration, TRADEX is not sensitive enough for incoherent-scatter measurements because of the extremely short pulsewidth and a high system noise temperature (see Table 1).

B. ALTAIR Data Summary

The ALTAIR data are summarized in Table 2. The day number, date, and start and end times (UT) are listed for each night of radar operation. A qualitative ESF activity index is also given in the righthand column. The letter A indicates an active night during which two or more strong backscatter plumes that extend well into the topside F layer were

Table 2

ALTAIR DATA SUMMARY

1977				
Day	Date, UT	Start Time, UT	End Time, UT	Activity Index*
225	8/13	1151	1228	Q
229	8/17	1017	1215	M
230	8/18	0837	1219	Q
232	8/20	0818	1231	M
233	8/21	0821	1232	Q
235	8/23	0830	1227	M
238	8/26	0929	1248	A
1978				
Day	Date, UT	Start Time, UT	End Time, UT	Activity Index
210	7/29	0817	1236	A
212	7/31	0827	1235	A
213	8/1	0953	1244	A
215	8/3	0818	1217	Q
218	8/6	0905	1050	Q
220	8/8	0816	1211	A
223	8/11	0818	1228	A
225	8/13	1004	1120	A
230	8/18	0738	1315	A
231	8/19	0730	1256	Q

Table 2 (Concluded)

1979				
Day	Date, UT	Start Time, UT	End Time, UT	Activity Index*
195	7/14	0725	1040	Q
198	7/17	0742	1320	A
199	7/18	0715	1040	Q
200	7/19	0730	1050	Q
203	7/22	0715	1040	A
204	7/23	0728	1120	M
205	7/24	0720	1210	A
1980				
Day	Date, UT	Start Time, UT	End Time, UT	Activity Index
183	7/1	0818	1227	A
184	7/2	0714	1229	A
185	7/3	0711	1231	A
186	7/4	0736	1227	A
190	7/8	0710	1233	A
191	7/9	0705	1404	A
192	7/10	0705	1214	M
193	7/11	0728	1218	M

*Q = Quiet.

M = Moderate.

A = Active.

observed. The letter M indicates a moderately disturbed night during which plumes were observed, but were not very strong in backscatter strength nor as extended in height as those observed on A nights. This second category also includes nights when one strong backscatter plume was observed but was preceded or followed by quiet or moderate activity. The letter Q indicates a quiet night during which plumes were not observed, although bottomside backscatter might have been observed.

The accumulated data base may be described as follows. Without accounting for periods of no data such as radar outages imposed radio-frequency silence during the arming of the rockets, ALTAIR was operated for 23 hours on 7 nights in 1977, for 36 hours on 10 nights in 1978, for 27 hours on 7 nights in 1979, and for 41 hours on 8 nights in 1980. (Analysis of the 1980 data set was not within the scope of this contract.) Scanning the list of activity indices, we find that ESF activity was considerably weaker in 1977 than in following years. The increase in ESF activity, particularly during 1980, is believed to be associated with solar activity.

III RESULTS

The results, summarized in this section, are presented in five parts. The first three subsections include results obtained from analysis of ALTAIR data collected from 1977 through 1979. The order of presentation is chronological, so that the reader can follow naturally our growth in understanding of ESF phenomena. As will become evident below, attention was originally centered on backscatter plumes (the most dramatic features in ALTAIR backscatter maps) and their spatial relationship to plasma bubbles (the most dramatic features found in satellite in-situ measurements). The focus of research on plumes and bubbles was also motivated by the fact that the collisional Rayleigh-Taylor instability, believed to be the source mechanism for bubble generation, is the gravitational analog of the gradient-drift instability; hence, the striations associated with bubbles must be analogous to those that form in a nuclear environment. During the course of research, it became evident (Section III-B) that the west wall of upwellings in the bottomside F layer was being structured via the gradient-drift instability, driven by an eastward neutral wind. This process is shown in this section to be the "seed" mechanism that initiates the development of bubbles and plumes.

In the fourth subsection, we summarize results from the 1979 TRADEX radar experiment in which we sought to extend the small-scale end of the fluctuation spectrum for equatorial irregularities.

In the fifth and final section, we present a detailed analysis of ALTAIR data which revealed the presence of a velocity shear (with altitude) in east-west plasma drift. It is this velocity shear that enhances the effectiveness of the gradient-drift instability.

A. 1977 ALTAIR Data Analysis

The 1977 ALTAIR data were first analyzed (under the Wideband project) to investigate the feasibility of extracting incoherent-scatter (IS) information out of ALTAIR backscatter data. Analysis of data collected in directions perpendicular and off-perpendicular to the geomagnetic field lines showed that IS returns were indeed measurable with ALTAIR (Tsunoda et al., 1978, 1979).[1,2] An important result of this analysis was the demonstration that backscatter measurements made with the radar beam directed perpendicularly to the geomagnetic field lines could also be used to measure the background F-layer electron density in the absence of ESF backscatter. Therefore, data recorded from field-perpendicular scans, in the absence of ESF backscatter, could be used to construct spatial maps of the background F layer. Furthermore, because of the patchy (i.e., spatially isolated) nature of ESF backscatter, estimates of background electron density could be made even during ESF activity.

The backscatter strength of ESF irregularities obtained at 155.5 MHz (VHF) and 415 MHz (UHF) with ALTAIR (and calibrated in terms of IS returns) was compared to that obtained with the Jicamarca 50-MHz radar (Woodman and LaHoz, 1976; Woodman and Basu, 1978). We found that ESF backscatter strength at 50 MHz is comparable to that obtained with ALTAIR at 155.5 MHz. That is, both radars observe maximum ESF backscatter strengths that are around 50 dB above IS, for an electron density of 10^6 el/cm^3. Considering that the wavelength dependence between the VHF and UHF returns obtained with ALTAIR can be represented by a power-law spectral index of 2.3, we would expect backscatter at 50 MHz to be 11 dB stronger than that at 155.5 MHz. [See Tsunoda et al. (1978, 1979)[1,2] for other details.]

At the time these results were obtained, little was known about the source mechanism for small-scale ESF irregularities--i.e., those with spatial wavelengths comparable to and less than the ion gyroradius (5.6 m for O^+ ions at a temperature of 1000 K). A reasonable scenario seemed to involve structuring at very large spatial scale sizes (up to a few hundred kilometers), followed by a cascade-like development of

smaller-scale structure produced by a hierarchy of plasma instabilities (e.g., Haerendel, 1973). A viable candidate for the initial structuring at the larger spatial scales was the collisional Rayleigh-Taylor instability (e.g., Scannapieco and Ossakow, 1976). At the small-scale end of the spectrum, Huba et al. (1978) proposed a plasma instability that involved high-frequency drift waves. The free energy for this instability was attributed to steep electron-density gradients associated with the walls of bubbles or large-scale irregularities.

At present, there is no known linear instability that can account for the 3-m structure that produces backscatter at 50 MHz (e.g., Huba and Ossakow, 1979). Rayleigh-Taylor and gradient-drift instabilities can produce structure with spatial scales approaching the ion gyroradius. At the small-scale end of the spatial fluctuation spectrum, the high-frequency drift-wave instability can account for spatial scales around the electron gyroradius and up to about 1 m. These results suggest that the weaker-than-expected backscatter at 50 MHz (in comparison to ALTAIR backscatter (Tsunoda et al., 1978, 1979)[1],[2] and to that expected from scintillation measurements (Woodman and Basu, 1978) is a consequence of the absence of a linear driver. The implication is that structure with a spatial wavelength around 3 m is produced by nonlinear coupling processes.

The first problem addressed under this contract was the spatial relationship between ALTAIR backscatter plumes and plasma bubbles. Woodman and Basu (1978) proposed that plumes, observed in their case with the Jicamarca radar, were tracers for the plasma bubbles that occurred in the nighttime equatorial F layer (e.g., Hanson and Sanatani, 1973). The first definitive result was obtained by comparing the east-west variations in total electron content (TEC) with the east-west locations of backscatter plumes (Tsunoda and Towle, 1979).[3],[4] [Inferences relating the two equatorial features had been made earlier (Tsunoda et al., 1978, 1979)[1],[2] by noting that plasma depletions did not seem to occur in regions between ESF backscatter where IS measurements were made.] By skin-tracking an east-west orbiting satellite at two frequencies (155.5 and 415 MHz), we were able to interpret the temporal variations in differential group delay as longitudinal variations in TEC. Plumes and depletions in TEC

were shown to be longitudinally collocated. This result was the first experimental evidence relating the two equatorial features.

B. 1978 ALTAIR Data Analysis

Pursuit of the spatial relationship between plumes and bubbles was continued in 1978 using IS measurements made with ALTAIR. Backscatter plumes were first detected and mapped spatially with a field-perpendicular scan. Five antenna beam positions were then selected (in real time) that intersected the geomagnetic field lines containing the strongest backscatter plume, but at off-perpendicular angles. Subsequent analysis of these data sets showed that backscatter plumes were indeed collocated with large depletions in F-layer plasma-density profiles (Tsunoda, 1980).[5] Thus, spatial collocation of plumes and bubbles inferred earlier using range-integrated TEC measurements (Tsunoda and Towle, 1979)[3,4] was shown to hold in both dimensions transverse to the geomagnetic field (Tsunoda, 1980).[5] Similar examples were also presented by Towle (1980).

Although general collocation occurred between plumes and bubbles, we also found that maximum backscatter strength appeared to be associated with the upper wall of bubbles (Tsunoda, 1980).[5,6] A similar tendency was found by Towle (1980). The spatial coincidence of strongest backscatter with the upper wall of bubbles is consistent with bubble development via the collisional Rayleigh-Taylor instability. Ossakow and Chaturvedi (1978) showed that bubbles driven by the Rayleigh-Taylor instability will steepen along its upper wall as they move upward through the F layer. The steep gradients along the upper walls presumably drive the high-frequency drift waves (Huba et al., 1978) that produce ALTAIR backscatter.

The fact that plumes are highly elongated (in altitude) structures that extend from the bottomside into the topside F layer suggests that bubbles are more like wedges than cylinders. That is, the plasma-depleted regions also are probably highly elongated in altitude and perhaps open-ended in the bottomside F layer. Numerical simulations of the collisional Rayleigh-Taylor instability (e.g., Zalesak and Ossakow, 1980)

predict the development of highly elongated bubbles. An alternative for plume interpretation is that the rising bubble is cylindrical in shape but leaves a wake of plasma-density irregularities behind it that scatters radio waves (Kelley and Ott, 1978). The results presented in Tsunoda (1980)[5] and other unpublished ALTAIR results suggest that the bubbles are elongated plasma-depleted regions. As will become evident later in this report, a source of structuring within the bubble along the side walls is an eastward neutral wind.

Incoherent-scatter measurements were also made to verify that plasma bubbles were actually depleted geomagnetic flux tubes (Tsunoda, 1980).[6] The description of bubbles usually assumes implicitly that they extend along geomagnetic field lines. This assumption is based more on theoretical grounds than on direct observational evidence. Using ALTAIR data collected in an elevation (or latitude) scan mode, we showed that a plasma bubble (up to 90% depleted) mapped along geomagnetic field lines over more than 10° of magnetic dip latitude.

While attempting to establish the spatial relationship of plumes and bubbles, both 1977 and 1978 ALTAIR data were also examined to characterize the temporal evolution of backscatter plumes (Tsunoda, 1980, 1981).[7,10] The temporal characterization (possible only with a steerable radar such as ALTAIR) was undertaken in order to be able to better predict plume behavior during the 1979 Kwajalein campaign. We found that individual plumes could be characterized by two phases--growth and decay. The two phases were distinguished by the time at which the upward growth velocity of plumes decreased, accompanied by a stabilization or decay in backscatter strength.

The key features found during the growth phase are: (1) plumes are generated primarily in the local time sector around F-layer sunset; (2) plumes develop where bottomside backscatter is locally elevated in altitude (i.e., altitude modulation or an upwelling in electron-density contours) rather than where bottomside backscatter is horizontally stratified; and (3) bottomside backscatter is often asymmetric in the east-west direction, with stronger backscatter occurring on the west wall of the upwelling. To account for these growth-phase characteristics, we

proposed a model (Tsunoda, 1980, 1981)[7,10] in which (1) the electron density is modulated by some means (e.g., atmospheric gravity waves) with bottomside backscatter acting as tracers for the resultant shape of constant electron-density contours, (2) there is an eastward neutral wind in the reference frame of the F-layer plasma drift, and (3) the steepening and structuring of plasma is initiated on the west wall of these upwellings via the gradient-drift instability (e.g., Linson and Workman, 1970) and with contributions from the collisional Rayleigh-Taylor instability at higher altitudes. Because the Rayleigh-Taylor instability is nothing more than the gradient-drift instability with a gravitational force term, the basic source mechanisms is a generalized gradient-drift instability.

C. 1979 ALTAIR Data Analysis

Focus for the analysis of 1979 ALTAIR data was placed on the measurements made during the nights of the two successful rocket launches, called PLUMEX I and II. The PLUMEX I rocket (launched on 17 July at 1231:30 UT) passed along the west side of a decaying (but still strong) backscatter plume before penetrating it just below rocket apogee. The PLUMEX II rocket (launched on 24 July at 0957:30 UT) passed along the east side of another strong backscatter plume but did not penetrate it.

The collocation of strongest ALTAIR backscatter with the upper wall of a plasma-depleted region, first shown in Tsunoda (1980),[5,6] was confirmed by the PLUMEX I rocket measurements (Szuszczewicz et al., 1980; Kelley et al., 1981).[9,13] In the data set presented by Tsunoda (1980)[5,6] and the one presented by Szuszczewicz et al. (1980)[9] the plumes were tilted west of vertical. If we assume that the plumes represent tracers for plasma-depleted regions, the assumed upper wall of the plasma "bubble" is actually the east wall of a wedge-shaped plasma-depleted region. This relationship was not clear in the data set presented by Tsunoda (1980)[6] because the IS measurements were made near the top of the plume where the bubble is expected to be located. In the PLUMEX I case, the rocket intersected the plume at a lower altitude, thus providing evidence that the plasma-depleted region is perhaps wedge-shaped and that structure is

associated with the east wall of the wedge. Zalesak et al. (1980) showed that the east wall would structure via the collisional Rayleigh-Taylor instability because there is a component of gravity directed antiparallel to the plasma-density gradient. This behavior is expected to dominate at high altitudes where the wind-driven gradient-drift instability is negligible compared to the gravity-driven Rayleigh-Taylor instability.

Evidence was found in the PLUMEX I and II rocket measurements that intense scintillation-producing irregularities are embedded in the west wall of the associated upwelling in the bottomside F layer. The most convincing results were those by Rino et al. (1981).[12] They showed that scintillations (measured by radio beacon transmissions from the PLUMEX I rocket) maximized in that region. In-situ probe measurements during the PLUMEX II rocket flight indicated that very little scintillation-producing structure was embedded in the east wall of the upwelling. These results are consistent with the structuring of the west wall (but not the east wall) of the upwelling by the gradient-drift instability driven by an eastward neutral wind.

Besides providing diagnostic support for the rocket measurements, ALTAIR data were analyzed to seek further verification for the plume generation model proposed by Tsunoda (1981).[7,10] Using IS measurements made during extended east-west scans with ALTAIR, we showed that wavelike modulation in plasma density occurs in the bottomside F layer prior to onset of ESF backscatter (Tsunoda and White, 1980, 1981).[11] Plumes were shown to grow from upwellings that developed from the crests of the wavelike modulation. Structuring was found to develop first along the west wall of each upwelling, as predicted by the plume generation model.

The requirement in the model (Tsunoda, 1980, 1981)[7,10] for an eastward neutral wind in the reference frame of the F-region plasma was believed to be satisfied by an F-region dynamo operating in the nighttime equatorial ionosphere (Rishbeth, 1971). But the velocity difference between the neutral gas and the plasma (i.e., the "slip" velocity) was not expected to be more than a few tens of meters per second because of close coupling of the F-region plasma to the neutral gas. Consequently, the structuring of the west wall of an upwelling was expected, but the

process was not expected to overwhelm the structuring pattern produced by the collisional Rayleigh-Taylor instability.

The discovery that a velocity shear (with altitude) in east-west plasma drift exists in the nighttime F layer (see Section III-E) has resulted in the enhancement of importance of the wind-driven gradient-drift instability in the equatorial ionosphere. That is, the velocity shear appears to produce a large slip velocity at low altitudes such that the rate of structuring in the west wall of an upwelling by the gradient-drift instability dominates the rate of structuring by the collisional Rayleigh-Taylor instability. Therefore, the west wall of an upwelling can be thought of as the "backside" (i.e., unstable region) of a large barium ion cloud.

D. TRADEX Data Analysis

As described above, ALTAIR was operated in support of the DNA rocket program to locate and track backscatter plumes into the rocket launch corridor. In 1979, the rockets were to be launched into these strong backscatter plumes. Yet very little was really known about the relationship of ALTAIR backscatter (i.e., 1-m and 36-cm irregularities) to larger-scale irregularities such as plasma bubbles and those that produce scintillations. Prior to ALTAIR observations, equatorial irregularities were believed to cut off around the ion gyroradius (5.6 m for O^+ ions at 1000 K). Since then, Huba et al. (1978) showed that high-frequency drift waves could produce the observed ALTAIR backscatter. The instability model predicted maximum irregularity growth rate near $kr_e \sim 1$ (where k is the wavenumber, and r_e is the electron gyroradius) and in plasma-depleted regions. Structure with this spatial wavelength would backscatter radio waves at 725 MHz.

In order to further characterize the irregularity scale-size regime below the ion gyroradius, the TRADEX radar was operated during Summer 1979 in conjunction with the ALTAIR radar. The objective of the experiment was to detect backscatter from 11-cm irregularities with TRADEX, and if backscatter was detected, to determine the wavelength dependence of backscatter by comparing TRADEX measurements with those by ALTAIR.

Backscatter was detected with TRADEX (Tsunoda, 1980).[8] The strongest returns observed were approximately 32 dB above IS levels (for an electron density of 10^6 el/cm^3). In comparison, the maximum backscatter strength typically observed at VHF (155.5 MHz) with ALTAIR is about 50 dB above IS levels. Therefore, backscatter from 11-cm irregularities is only about 20 dB below that observed for 1-m irregularities.

For a more quantitative analysis, we computed the backscatter volume reflectivity from measurements made simultaneously by ALTAIR and TRADEX (Tsunoda, 1980).[8] We found that the wavelength dependence varied from $\lambda^{2.3}$ between VHF and UHF (415 MHz), to $\lambda^{1.3}$ between UHF and L band (1320 MHz). Although more data must be analyzed to confirm this preliminary result, the flattening of the fluctuation spectrum between UHF and L band is consistent with the high-frequency-drift-waves theory, which predicts strongest backscatter around 725 MHz.

E. Evidence of a Velocity Shear in Bulk Plasma Motion Associated with the Post-Sunset Rise of the Equatorial F Layer

1. Introduction

Until recently, little attention has been given to the possibility that the electrodynamics of the equatorial F layer might depend on altitude. Bulk F-layer plasma motion has in the past been attributed solely to the E-region dynamo driven by tidal neutral winds (e.g., see Rishbeth, 1977, for review). Any large-scale electric field that is set up in the E region is communicated to the equatorial F layer along geomagnetic-field lines; therefore, the altitude variation in F-region plasma motion is a direct mapping of the latitudinal variation in the E-region electric field. To date, there are no indications of rapid latitudinal variations in the E-region electric field.

More recently, Rishbeth (1971) proposed that an F-region dynamo operates under nighttime conditions when the E layer no longer can prevent F-region polarization electric fields from developing. An eastward neutral wind in the equatorial F region would drive an upward-directed ion Pedersen current. Because electrons are confined to motion along

geomagnetic-field lines, a polarization electric field will set up as a result of the charge separation. The electric field, if not shorted by a conducting E layer, will drive the F-layer plasma eastward.

In the simplest case, the F-region dynamo electric field will depend on altitude if (1) the E layer has a finite conductivity, and (2) the F-layer Pedersen conductivity (integrated along geomagnetic-field lines) depends on altitude (Zalesak et al., 1980). If the E-layer conductivity is zero, the F layer will become fully polarized and drift identifically with the neutral wind, independent of altitude (e.g., Rishbeth, 1971). If, however, a finite Pedersen current is allowed to flow in the F layer with closure through a finitely conducting E layer (via field-aligned currents), the polarization electric field will be proportional to the F-layer Pedersen conductivity. The altitude variation in the electric field will, therefore, depend on the Pedersen conductivity profile. The second requirement, that the F-layer Pedersen conductivity is altitude-dependent, is obviously satisfied.

The first demonstration that the bulk-plasma motion might depend on altitude, particularly around E-region sunset and during the premidnight sector, was presented by Heelis et al. (1974). Their model consisted of (1) the E-region dynamo driven by tidal winds and F-region field-aligned currents, (2) the coupling of electric fields from E to F regions (along geomagnetic field lines), (3) the F-region dynamo driven by both the neutral wind and E-region electric fields, and (4) the mapping of F-region field-aligned currents down to the E region (along geomagnetic field lines). Their iteration scheme for a self-consistent solution consisted of initially assuming the field-aligned current to be zero. The tidal electric field was then used to compute F-region ion motion and current flow transverse to the geomagnetic field. The requirement that $\nabla \cdot \vec{j} = 0$ was used to compute the field-aligned current. The E-region electric field was then recomputed allowing for the newly computed field-aligned current. By this method, Heelis et al. (1974) showed that a velocity shear (with altitude) in the east-west plasma motion existed during this period. The velocity shear consisted of a residual westward flow at low altitudes and an eastward flow at high altitudes.

Experimental evidence supporting the theoretical model prediction of a velocity shear by Heelis et al. (1974) has, thus far, been very limited. Haerendel (1980) collected drift measurements of barium-ion-cloud releases in the equatorial ionosphere and interpreted those drifts in terms of a velocity shear in plasma flow. Kudeki et al. (1980) used a radar interferometry technique, applied to the Jicamarca radar, to show that a velocity shear existed in the east-west drift of equatorial spread-F (ESF) irregularities in the lower F layer. And, Tsunoda (1981)[10] presented an example of velocity shear in ESF irregularity drift found in time-sequenced backscatter maps obtained with the ALTAIR radar (Tsunoda et al., 1979;[2] Towle, 1980). On the other hand, Woodman (1970, 1972), using the Jicamarca radar, found no evidence that either the east-west or vertical motions of the equatorial F-region plasma depended on altitude.

In this section, we present additional evidence that F-region plasma flow after E-region sunset is characterized by a velocity vortex pattern. Thw two-dimensional plasma flow pattern was constructed from ESF backscatter and incoherent-scatter data collected with ALTAIR on 24 July 1979. ALTAIR measurements were made over a 1-1/2 hour period on a single night, in contrast to the barium-cloud data used by Haerendel (1980), which were collected over several years. The results verify the importance of the F-region dynamo in equatorial plasma electrodynamics and allow new interpretation of ESF backscatter generation processes.

2. Experimental Considerations

The ALTAIR radar and its system characteristics have been described in earlier papers (e.g., Tsunoda et al., 1979;[2] Towle, 1980); therefore, a detailed description is not repeated here. Instead, we briefly summarize the pertinent radar parameters and describe modifications in ALTAIR operation that allowed collection of the data reported in this paper.

ALTAIR is a dual-frequency radar that operates simultaneously at 155.5 MHz (VHF) and 415 MHz (UHF). Its peak power and effective antenna aperture together allow incoherent-scatter measurements to be made

at both radar frequencies. Although data were collected for this experiment at both frequencies, we present only data collected at 415 MHz. This choice was made because the radar is slightly more sensitive at UHF (using a 40-μs pulse) than at VHF, and because ESF backscatter is about 10-dB weaker at UHF than at VHF. Consequently, the use of UHF data provides a more accurate measure of the ionospheric electron-density distribution.

The experiment consisted of scanning the ALTAIR beam repeatedly in the east-west direction. The scans were all made with the radar beam directed perpendicular to the geomagnetic field at F-region altitudes. As shown by Tsunoda et al. (1979),[2] these scans provide incoherent-scatter measurements of the F-layer electron density in the absence of ESF irregularities, and map the ESF irregularities under disturbed conditions. Therefore, by operating ALTAIR before and during the development of ESF, it was possible to map the ionospheric conditions that just preceded the development of ESF structure.

The scans differed from those previously reported (Tsunoda et al., 1979;[2] Towle, 1980) in that they were continuous (rather than discrete) and significantly expanded in east-west extent. The continuous scan allowed for improved angular resolution. The expanded angular width of 120° (compared to 45° and 72° used previously) provided an east-west coverage of over 1200 km (compared to 600 km) at an altitude of 400 km.

3. Results

In this section we extract the east-west plasma drift as a function of altitude and time from a sequence of ALTAIR ESF backscatter maps. This information is then combined with the vertical plasma drift (assumed independent of altitude) obtained from ALTAIR incoherent-scatter measurements (and ionosonde data) to construct a two-dimensional plasma flow pattern for the equatorial F-layer around E-region sunset. Although irregularity drift (i.e., that of ESF backscatter), in general, is not identical to bulk plasma motion, the differences are usually small enough that the qualitative flow pattern that is derived is reasonably descriptive

of the real flow pattern. On the other hand, the vertical speed of ESF irregularities is not a reliable tracer of vertical F-layer motion. The growth velocity of backscatter plumes, for example, can be several times the vertical velocity of the F layer (Tsunoda, 1981).[10] For this reason, we have resorted to estimating vertical velocities from incoherent-scatter (and ionosonde) measurements. Vertical plasma transport estimated from profile displacements as a function of time, although also subject to error (because loss processes and distortion of the profile must be accounted for), is sufficiently accurate for our purposes.

The sequence of ALTAIR backscatter maps from which the east-west plasma drift is extracted are presented in Figure 1. The data set was obtained on 24 July 1979, from 0745 to 0915 UT (1855 to 2025 local solar time). A detailed description of the same ALTAIR data set has already been presented by Tsunoda and White (1980).[11] We therefore refer the reader to that paper for a general description and other details, and focus here on the plasma electrodynamics. The maps in Figure 1 are stacked with the scan made earliest in time placed at the bottom and that made last placed at the top. The contours represent constant backscatter strength (after range-squared correction) referenced to incoherent-scatter levels. That is, the weakest backscatter contour (dashed curve) corresponds in strength to equivalent incoherent scatter from an electron density of 10^5 el/cm^3. Other contours are given in 10-dB increments above this value. (Although the contours are not labeled, the stronger backscatter regions are, in most cases, concentric with the weaker ones.)

To determine the east-west drift of F-region plasma as a function of altitude and time, we used the east-west displacement of various backscatter features in the maps in Figure 1 and divided the displacements by the corresponding time differences between successive measurements of the same feature. To obtain velocity estimates at various altitudes, we used features such as electron-density contours (e.g., dashed curve) in the bottomside F layer, bottomside ESF backscatter, and plume backscatter. The selected backscatter features are shown in Figure 1 connected by straight line segments between maps and labeled with letters a through m.

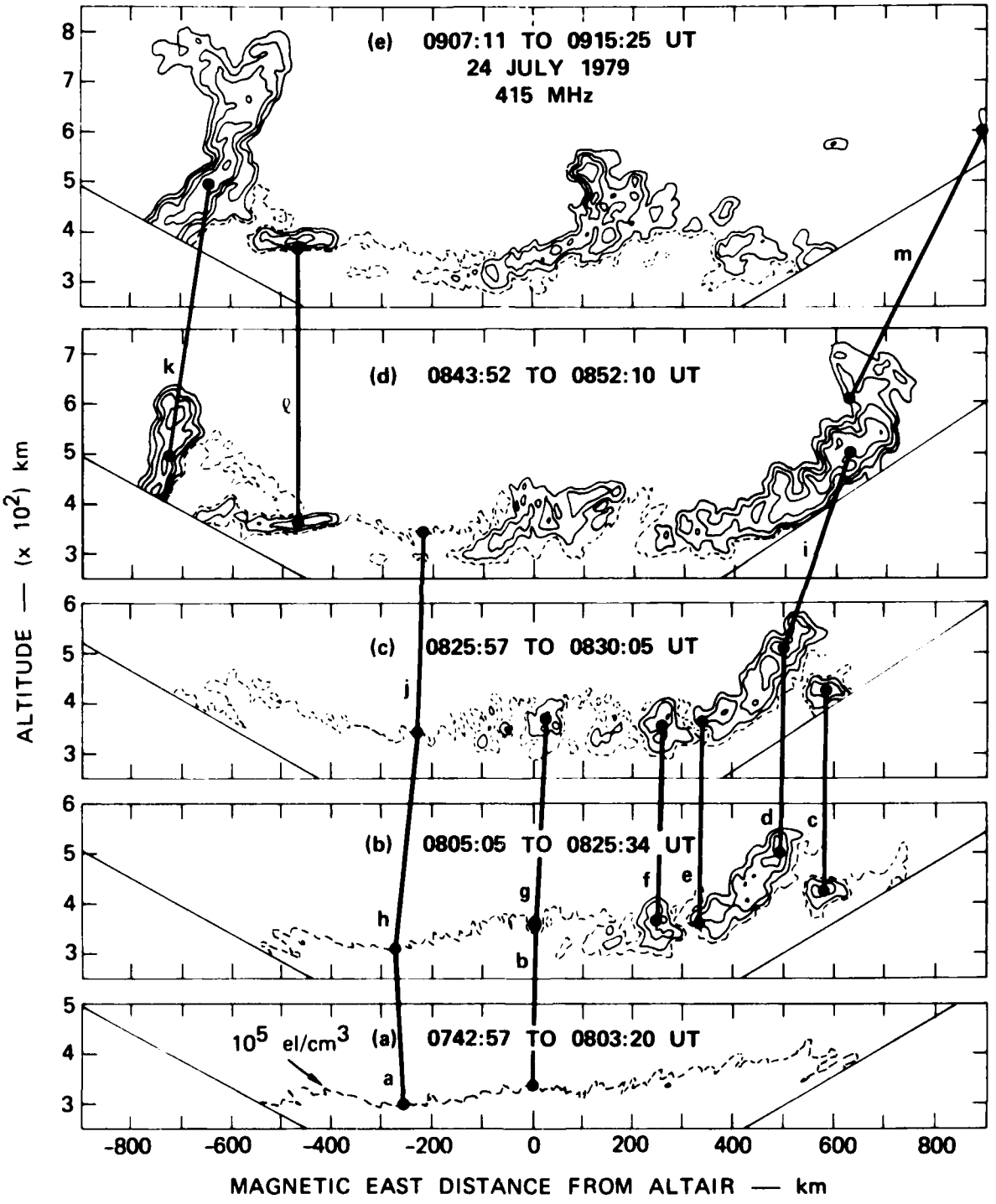

FIGURE 1 SEQUENCE OF ALTAIR BACKSCATTER MAPS USED TO ESTIMATE EAST-WEST PLASMA DRIFT vs ALTITUDE AND TIME

The plasma drift velocities extracted from Figure 1 are plotted in Figure 2, as a function of time. The horizontal bars bracket the time over which each velocity measurement was made. Each bar is labeled with a letter corresponding to the feature labeled in Figure 1. For purposes of discussion, the high-altitude velocity estimates are drawn with solid bars and the low-altitude velocity estimates are drawn with broken bars. The altitudes corresponding to the cluster of bars in Figure 2 labeled c through f are less clear. Bars e and f correspond to low-altitude velocity estimates, Bar c corresponds to an intermediate-altitude velocity estimate, and Bar d to a high-altitude velocity estimate.

At first glance, the plasma drift velocities derived from backscatter features appear in Figure 2 to show large scatter with westward or small eastward drifts at earlier times, and both large and small eastward drifts at later times. Two trends are, however, apparent after closer examination. The trend associated with the low-altitude measurements starts with westward or small eastward drifts at early times, followed by an increasing eastward velocity shortly after E-region sunset ($\sim$ 0800 UT), and a decreasing eastward drift thereafter. The trend associated with high-altitude measurements begins at a later time (the presence of plumes is required for measurement) and increases in eastward velocity as a function of time. The striking feature is the divergence of the high- and low-altitude velocities as a function of time beginning around 0815 UT. The measurements that indicate the presence of a velocity shear with altitude are (1) the near-simultaneous measurements of a large eastward velocity at high altitudes and a small eastward velocity at low altitudes (i.e., Bars i and j, and Bars m, k, and ℓ, in Figure 2), and (2) the measurement of an actual westward drift at low altitudes (Bar a).

For comparison, we have included in Figure 2 the mean horizontal bulk plasma drift (dashed curve) determined by Woodman (1972) using the Jicamarca incohrent-scatter radar. The curve is a hand-smoothed running average of composite data collected over 12 days, and probably representative of the altitude range from 300 to 450 km, near the peak

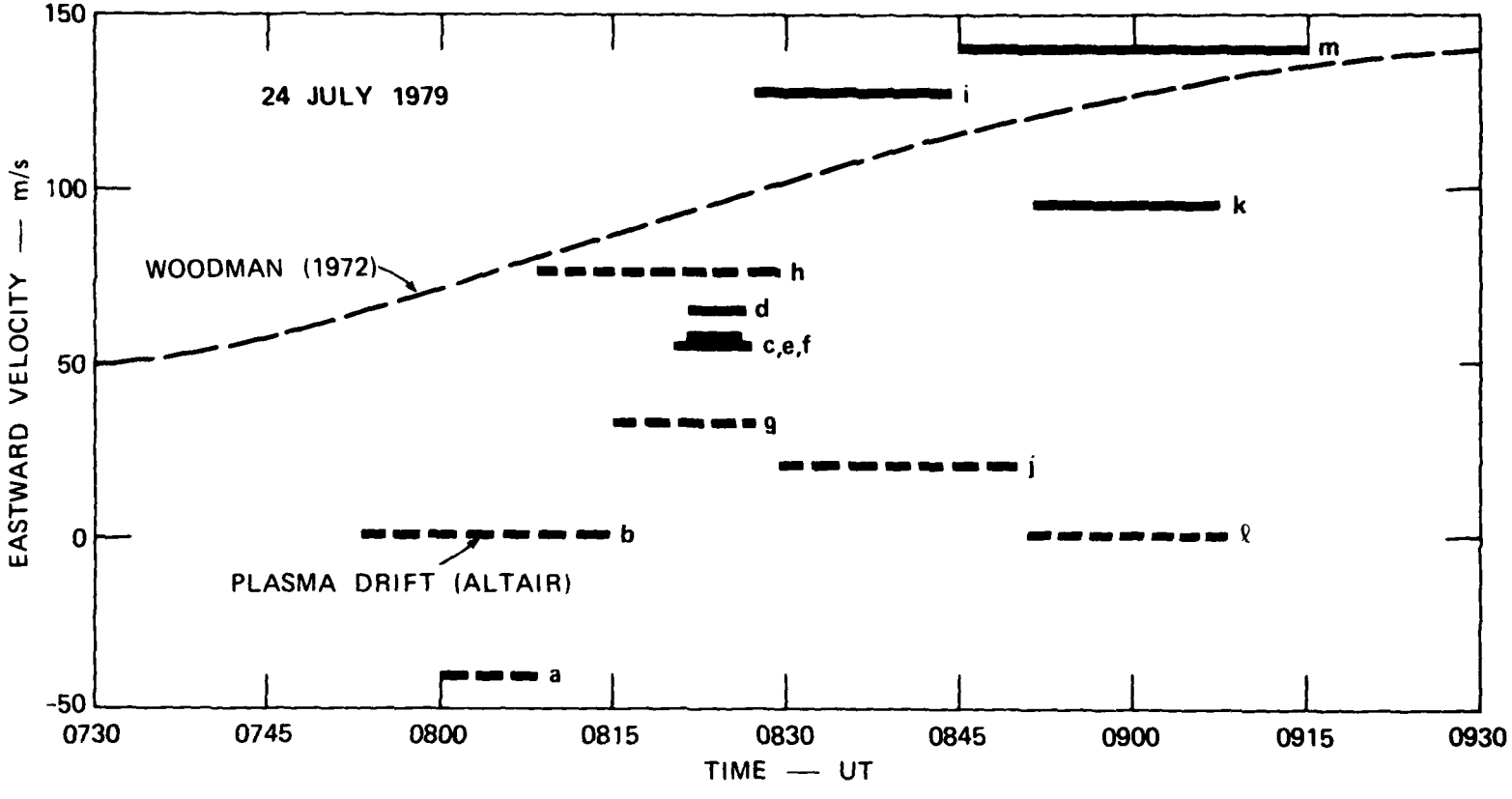

FIGURE 2 EASTWARD PLASMA DRIFTS (HORIZONTAL BARS) DERIVED FROM FIGURE 1 AND FROM JICAMARCA RADAR MEASUREMENTS PLOTTED vs TIME

of the F layer. Woodman's curve is 50 m/s larger than our low-altitude results at early times and agrees well with our high-altitude results at late times. (The scatter of the high-altitude velocity estimates is about ±30 m/s about Woodman's curve.)

A two-dimensional plasma-flow pattern can be constructed if we reorder the east-west velocity estimates shown in Figure 2 as a function of altitude and time and include the vertical velocity component. The variation of the vertical velocity, obtained from incoherent-scatter and ionosonde measurements, is shown plotted as a function of time in the upper panel of Figure 3. The upward velocity was nominally 40 m/s for times prior to 0815 UT and virtually zero for the remaining period of interest. The zero vertical velocity is based on estimates of altitude changes in the bottomside F-layer contours in the last two maps in Figure 1. Ionograms taken during this period also suggest the existence of a stable F layer between 0815 and 0930 UT.

The model of the bulk plasma motion as a function of altitude and time is shown in the lower panel of Figure 3. The east-west and vertical velocity components have been combined and replotted at the altitude and mean time of measurement; the velocity vector is represented by the length and direction of the arrows. Stream lines have been schematically added to suggest a flow pattern that is consistent with the measurements. The westward and upward flow at low altitudes is suggested by Points a and b. The reversal to an eastward flow at higher altitudes and later times is suggested by the measurements between 0815 and 0845 UT. Finally, the closure of the stream lines at later times by a downward plasma motion is inferred from the fact that the F layer is known to descend within a few hours after sunset.

The stream lines, as we have drawn them in Figure 3, suggest that the east-west flow reverses at an altitude of about 300 km. The velocity shear with altitude, however, is not evident in the measurements until after around 0830 UT. The length and direction of the arrows shown in Figure 3, between 0815 and 0830 UT, is nearly uniform from the 330-km to the 500-km altitude. After 0830 UT, the differences in the

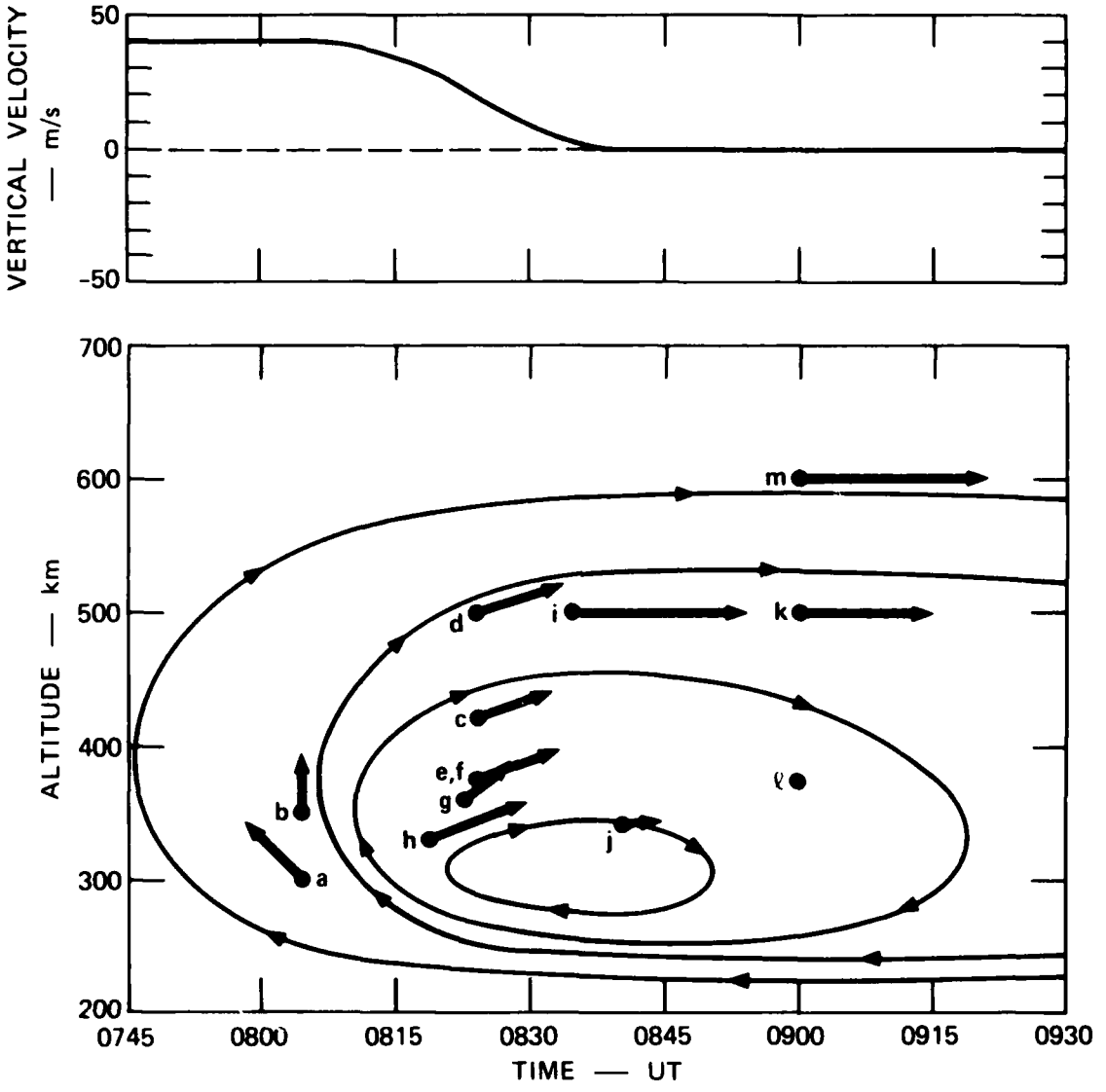

FIGURE 3 F-REGION PLASMA FLOW PATTERN (LOWER PANEL) INFERRED FROM THE EAST-WEST PLASMA DRIFT RESULTS IN FIGURE 2 AND FROM THE OBSERVED VERTICAL PLASMA MOTION (UPPER PANEL)

velocities are significant. This result indicates that the velocity shear developed shortly after E-region sunset (~ 0800 UT), which is consistent with the concept that the F-region dynamo produces the velocity shear.

Comparing our results to the model predictions by Heelis et al. (1974), we find good agreement in the time of velocity-shear development, but not in the altitude where the horizontal velocity reverses. Heelis et al. (1974) showed (see their Figure 9) a buildup in velocity shear sometime between 1800 and 2300 local times, as compared to our observation for shear onset time of 0830 UT, or 1940 local solar time. The altitude of horizontal velocity reversal, however, was located at around the 220-km altitude, as compared to our 300-km altitude. This discrepancy is discussed in the next section.

4. Discussion and Conclusions

We have shown that by using the east-west drift of ESF irregularities as tracers for bulk plasma motion and combining this information with altitude displacements of F-layer electron-density profiles, we can construct a two-dimensional, F-region plasma-flow model. Furthermore, the flow pattern constructed from data collected around E-region sunset resembled a vortex. The vortex flow pattern in Figure 3 is qualitatively consistent with the measurements published by Woodman (1970, 1972). By combining his east-west and vertical velocity measurements, we obtain a velocity vector that rotates clockwise from westward and upward during the day, to eastward and downward during the night. This pattern of velocity vector rotation agrees with the vortex model in Figure 3 at an altitude of around 400 km, the approximate altitude of his measurements.

A discrepance was found, however, in the more quantitative comparison between Woodman's curve of mean east-west plasma drift (Woodman, 1972) and our results in Figure 2. As discussed in the previous section, Woodman's curve was approximately 50 m/s higher than our low-altitude velocity estimates at early times. This difference can be attributed to the fact that Woodman's curve reverses from westward to eastward drift

at a much earlier time (~ 1630 local time) than was observed in the ALTAIR results (see Figure 2). Similar differences were noted by Balsley (1973) when he compared the same Jicamarca results with various other measurements. All the other measurements (which included barium-ion-cloud drift and spaced-receiver drift techniques) showed reversal times close to 2000 local time, which is in reasonable agreement with our results. Because the east-west drift shows a very consistent behavior from day to day (Woodman, 1974) and appears to be virtually independent of season, solar cycle, and magnetic activity (Fejer et al., 1979), the difference in reversal time cannot be easily attributed to those factors.

The discrepancy in the shear reversal altitude (mentioned in the previous section) between our results and the model of Heelis et al. (1974) can probably be attributed to their choice of ionospheric model parameters. Heelis et al. (1974) used an electron density profile with a peak altitude that ranged from 350 km down to 300 km. The peak of the F layer for our data set was closer to an altitude of 500 km (Tsunoda and White, 1980).[11] Other factors being equal, this difference would shift their velocity shear pattern upward in altitude. Another factor, not included in their model computation, is the plasma density distribution governed by the F-region continuity equation (which must be solved simultaneously with the dynamical equations). Tsunoda (1980)[6] has shown that the plasma density distribution can vary significantly in the pre-midnight sector with latitude and altitude.

Having demonstrated that a velocity vortex develops in F-region plasma flow around E-region sunset, we now consider its impact on ESF backscatter plume development. As seen in Figure 1 and described by Tsunoda and White (1980),[11] the same data set used here corresponded to a time during which ESF backscatter was in its growth phase (Tsunoda, 1981).[10] Tsunoda (1981)[10] proposed a model for backscatter plume generation that called for an eastward neutral wind to blow through the west wall of local altitude-modulated regions in the bottomside F layer. (The wave structure seen in the bottom panel of Figure 1 is an example of this altitude modulation.) The effectiveness of the model depends on the magnitude of the velocity difference between the neutral gas and

the F-region plasma. Tsunoda (1981)[10] found evidence of velocity shear in one of his examples and speculated that a velocity shear would act to enhance the effectiveness of his model. His speculation is partly verified here by the demonstration that a velocity shear does exist. Verification of his model is completed in a future paper in which we show that the neutral wind was indeed large and directed eastward during the same time period.

Another question into which we now have better insight is, what is the source mechanism for "valley spread F?" Woodman and La Hoz (1976) observed backscatter from low altitudes corresponding to the valley region of the ionosphere. Tsunoda et al. (1979)[2] presented an example of valley spread F observed with ALTAIR. The radar signature for valley spread F, at least as observed with ALTAIR, can be seen in the top two maps in Figure 1. The radar signature is a horizontally oriented backscatter layer that protrudes from the east wall of the west crest (i.e., the feature labeled ℓ). In this example, it is located at an altitude of about 375 km. In the example presented by Tsunoda et al. (1979),[2] the backscatter layer was at a lower altitude, around 225 km. These features can be explained by the "pulling" of plasma out of the east wall of an altitude-modulated region by the velocity shear.

IV DISCUSSION AND CONCLUSIONS

The ALTAIR and TRADEX results summarized in the previous section indicate that ESF irregularities with spatial wavelengths less than the ion gyroradius (approximately 6 m in the nighttime equatorial F layer) are spatially collocated with plasma bubbles--i.e., local depletions in F-region plasma density. This spatial collocation is consistent with the hypothesis that the lower-hybrid-drift (LHD) instability is the source mechanism for these small-scale, field-aligned irregularities (Huba et al., 1978; Sperling and Goldman, 1980; Huba and Ossakow, 1981). For example, the LHD instability requires a mean plasma density of less than 10^5 el/cm^3 for gradient scale lengths around 50 m (Sperling and Goldman, 1980).

By interpreting ESF backscatter plumes mapped by ALTAIR in terms of plasma-depleted regions we were able to follow, for the first time, the temporal evolution of plasma bubbles. Plasma bubble development in the nighttime equatorial ionosphere was shown to generally follow the numerical simulations of the nonlinear, collisional Rayleigh-Taylor instability (e.g., Ossakow et al., 1979; Zalesak and Ossakow, 1980). That is, bubbles were generated in the bottomside F layer and developed upward, penetrating into the topside F layer. A more realistic description of plasma bubble evolution, however, appears to require the effects of (1) an eastward neutral wind in the reference frame of the F-region plasma, (2) a velocity shear (with altitude) in the east-west plasma drift, and (3) a generalized gradient-drift instability that includes the Rayleigh-Taylor instability as the gravitational force term in the dispersion relation.

A descriptive model of plasma bubble evolution that incorporates the above factors is presented in Figure 4. A plasma bubble is initiated in the bottomside F layer where there is a local altitude modulation (or upwelling) in the plasma-density contours. Such an upwelling is shown in Figure 4(a). The development of the upwelling, shown in Figure 4(b),

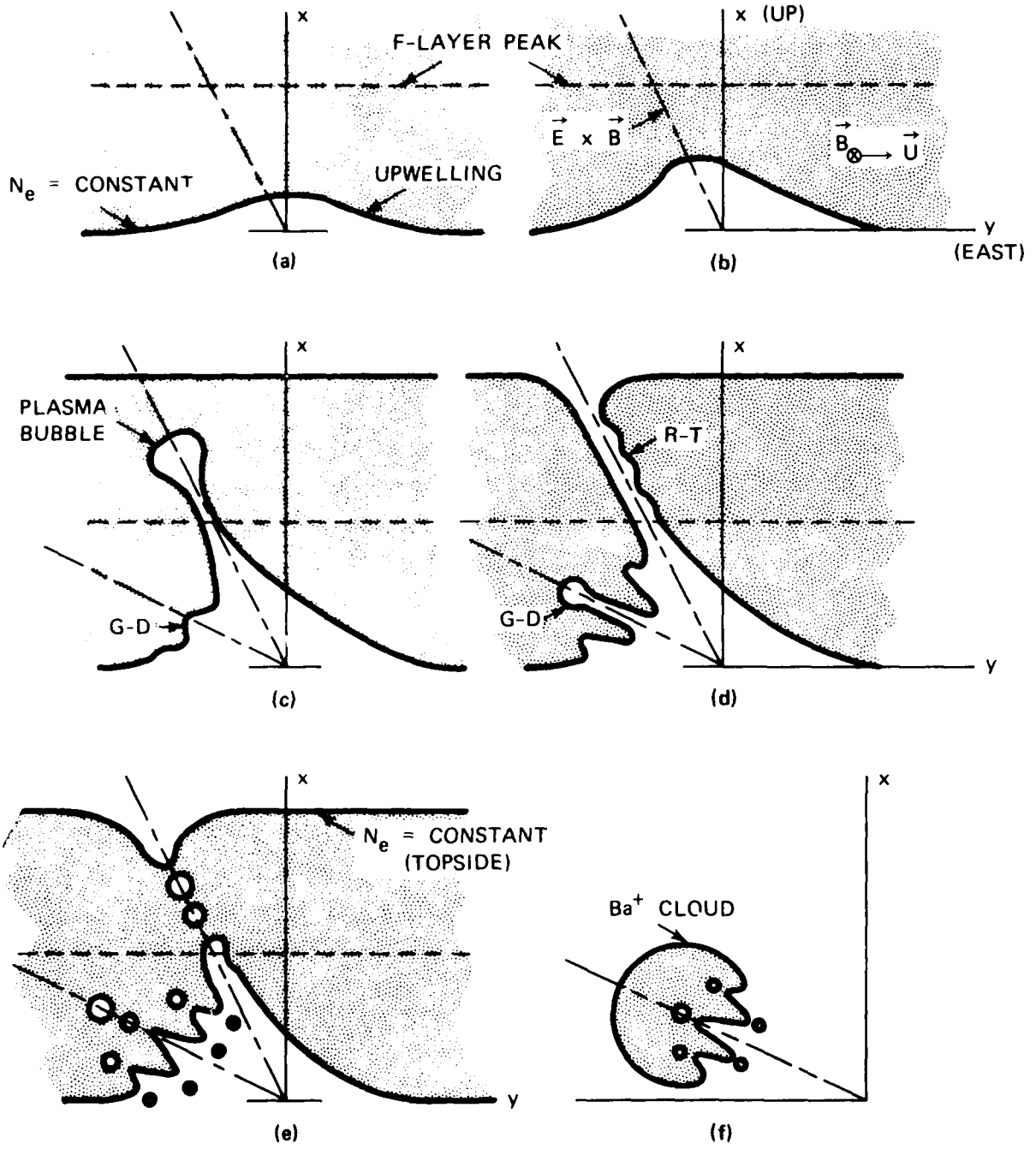

FIGURE 4 DESCRIPTIVE MODEL OF PLASMA STRUCTURING IN THE EQUATORIAL F LAYER PRODUCED BY THE GRADIENT-DRIFT AND COLLISIONAL RAYLEIGH-TAYLOR INSTABILITIES

is usually upward and westward. The tilt angle is dependent on the ratio of the velocity components in the x (up) and y (east) directions. The upward velocity component is proportional to g/ν_{in} (where g = gravitational acceleration, and ν_{in} = ion neutral collision frequency) and an eastward electric field, if any. The westward velocity component is proportional to the relative velocity between the neutral gas and the F-region plasma. A plasma bubble eventually develops from the peak of the upwelling and penetrates into the topside of the F layer, as shown in Figure 4(c). The plasma bubble will continue to push upward until the plasma density inside the bubble becomes identical to that outside the bubble, as shown in Figure 4(d).

Plasma structuring occurs not only in the form of the bubble but also along the west wall of the upwelling, as shown in Figure 4(c). The structure there (labeled G-D) is produced via the gradient-drift instability by an eastward neutral wind blowing through the west wall of the upwelling. The structuring rate is rapid at lower altitudes where the plasma drift is small or even westward (see Section III-E), thus resulting in a large slip velocity. (The direction of structure alignment differs at low altitudes from the plasma bubble because of the velocity shear with altitude.) The continued structuring of the west wall is shown in Figures 4(d) and 4(e). Structure can also develop along the east wall of the plasma bubble at high altitudes. Structuring there (labeled R-T) occurs via the collisional Rayleigh-Taylor instability because g/ν_{in} is large and there is an upward component in plasma density gradient. Because the west wall is a direct analog of barium ion clouds, we expect striations in the form of "rods" to develop through a "pinching off" process, as shown in Figure 4(e).

Evidence that the slip velocity is large along the west wall of an upwelling was presented in Section III-E. We showed that the difference in plasma drift velocity between high and low altitudes can be on the order of 100 m/s. The slip velocity is also of that order because the neutral wind is slightly faster than the high-altitude plasma drift (Rishbeth, 1971). If we assume the low-altitude F-region plasma to be motionless (as in the example presented in Section III-E), the slip velocity will be

that of the neutral wind. Sipler and Biondi (1978) have shown that the F-region neutral wind velocity is above 100 m/s for two to four hours in the premidnight sector.

The direct analogy found between the west wall of an upwelling in the equatorial F layer and a barium ion cloud suggests that some of the nuclear phenomenology questions addressed with barium ion cloud experiments can also be investigated (perhaps to advantage) at the equator. For example, a problem of DNA interest is the "freezing phenomena" observed in barium ion cloud striations. The problem is, why do gradient-drift-driven structures not continue to bifurcate beyond a certain minimum scale size? A direct approach to the solution is to observe striation development over a long period of time.

A comparison of available observation time for barium cloud experiments and ESF experiments shows that striation development can be viewed for a longer period of time with ESF experiments. The longest optical observation of barium ion cloud structure lasted less than two hours after the time of release (D. R. McDaniel, personal communication, 1981). In the ESF case, because of the confined direction of movement (i.e., eastward), all structure that develops to the west of the observing site will eventually pass overhead of that site. Therefore, ESF structure of any age can be observed from one site. Because the neutral wind exceeds 100 m/s for a period of 2 to 4 hours on any given night, we can expect strongly driven gradient-drift structures to evolve over a similar period of time. Consequently, we would expect to be able to observe striations in the west walls of upwellings that are as old as 4 hours.

In order to estimate the age of an ESF structure, we would want to monitor its time evolution. We have already shown that this is possible with ALTAIR. In 1979, ALTAIR was scanned over a 120° angular sector, equivalent to a ±600 km east-west coverage at F-region altitudes. At 100 m/s eastward drift, a plume that develops 600 km west of ALTAIR will arrive over ALTAIR 100 minutes later. The structure in the west wall of the associated upwelling should be at least 100 minutes old, comparable to the longest observation period for ion cloud structure.

Estimates of the age of older structure can be made by placing another backscatter radar to the west of ALTAIR. For example, if a radar is located at Eniwetok, 500 km west of ALTAIR, the sector coverage can be extended from 600 km to 1000 km (or more) west of ALTAIR. At this distance, the plumes detected 500 km west of Eniwetok will arrive over ALTAIR 167 minutes later. Selection of radar sites further to the west would result in estimates of older striations. If an accurate measurement of striation age is not required, we can estimate the age of the striation from its local time of appearance. This is possible because plumes are typically generated around E-region sunset. For example, plumes arriving over ALTAIR in the midnight sector should be approximately 4 hours old. An example of such a plume would be that into which the PLUMEX I rocket was launched. In fact, spectral characteristics obtained from the rocket in-situ measurements contain features that might be associated with "freezing" (Rino et al., 1981).

The results discussed above can also be used to determine the spatial relationships of plasma bubbles, ALTAIR backscatter, and scintillation-producing irregularities. We already know that ALTAIR backscatter is spatially coincident with plasma bubbles. Or, the backscatter is associated with steep gradients found in low-plasma density regions--e.g., bubbles, walls, or larger-scale irregularities embedded in the bubble volume. The relationship to be determined, then, is that between ALTAIR backscatter (or bubbles) and scintillation-producing irregularities.

We begin the analysis by assuming that the scintillation-producing irregularities are cylindrical rods with a Gaussian plasma density variation transverse to the geomagnetic field. If we define the gradient scale length as $L \equiv N(\nabla N)^{-1}$, L is equal to one-fourth the transverse (1/e) width, W, of the rod. The scale size that dominates intensity scintillation is close to the Fresnel radius. For a geostationary satellite, the Fresnel radius at 300 MHz is 178 m. For the Wideband satellite, the corresponding Fresnel radius is 150 m. The gradient scale length for both cases is about 50 m. Therefore, as noted earlier, the LHD instability requires a mean plasma density of less than 10^5 el/cm^3 for a gradient scale length of around 50 m.

On the basis of the above arguments, we would expect ALTAIR backscatter to be associated with scintillation-producing irregularities embedded in a mean plasma density of 10^5 el/cm^3, or less. This restriction implies spatial coincidence of backscatter and scintillation-producing irregularities only along the bottomside F layer and within the upwelling. Scintillation-producing irregularities embedded within the west wall of the upwelling in higher plasma density regions will not be accompanied by ALTAIR backscatter. Also, because scintillations will be proportional to the background plasma density, the stronger scintillations should be associated with the higher plasma density regions. On this basis, a careful examination should reveal that scintillations are displaced to the west of backscatter regions near the west wall of an upwelling.

In conclusion, the ALTAIR project has unscrambled the apparent complexities of equatorial spread F and demonstrated that the collisional Rayleigh-Taylor instability is a dominant source mechanism initiating the structuring process, in the form of plasma bubbles. The analysis has also revealed that the west wall of upwellings originating in the bottomside F layer is directly analogous to barium ion clouds and that the structuring there is dominated by the gradient-drift instability, driven by the neutral wind. With these discoveries as a foundation, it is now possible to intelligently pursue DNA-relevant problems in nuclear phenomenology--in particular, structuring processes driven by the gradient-drift instability.

There are certain advantages to equatorial spread F as a natural simulator of gradient-drift-driven structures. As discussed above, the "freezing" phenomenon observed in barium clouds is more amenable to study at the equator. Because the disturbance is naturally produced, a rocket need not be dedicated to seeding, as in the barium case. As a result, only rockets with diagnostic payloads are required. The multiple occurrence of bubbles (or radar plumes) on a given night and their reoccurrence from night to night would allow selective criteria that would ensure program success.

The role of ESF phenomenon as a testbed for investigating gradient-drift-driven structures should actually be thought of as complementing

the role of barium clouds. For example, barium clouds are usually only a few kilometers in size. Equatorial upwellings are a few hundred kilometers in size. Also, equatorial spread F is always associated with small E-region conductivities. Barium clouds can be coupled to E regions of varying conductivities by selecting the location of the releases. Equatorial spread F involves entire magnetic flux tubes and can therefore be considered as two-dimensional structures. On the other hand, barium clouds are local perturbations that are perhaps more three-dimensional in nature. Differences observed in structure development in the two cases would help us to further understand the ramifications of gradient-drift-driven structures in a nuclear environment.

REFERENCES

1. Balsley, B. B., "Electric Fields in the Equatorial Ionosphere: A Review of Techniques and Measurements," J. Atmos. Terr. Phys., 35, 1035, 1973.

2. Christiansen, R. M., "Preliminary Report of S-Band Propagation Disturbance during ALSEP Mission Support (19 November 1960-30 June 1970)," NASA Report X-861-71-239, Goddard Space Flight Center, Greenbelt, MD, 1971.

3. Craft, H. D., Jr., and L. H. Westerlund, "Scintillations at 4 and 6 GHz Caused by the Ionosphere," paper presented at AIAA 10th Aerospace Sciences Meeting, San Diego, CA, 1972.

4. Crampton, E. E., Jr., and W. B. Sessions, "Experimental Results of Simultaneous Measurement of Ionospheric Amplitude Variations of 136 MHz and 1550 MHz Signals at the Geomagnetic Equator," NASA Report X-490-71-54, Goddard Space Flight Center, Greenbelt, MD, 1971.

5. Fejer, B. G., C. A. Gonzales, D. T. Farley, R. F. Woodman, and C. Calderon, "F-Region East-West Drifts at Jicamarca," J. Geophys. Res., in press, 1981.

6. Haerendel, G. "Theory of Equatorial Spread F," preprint, Max-Planck-Inst. für Phys. und Astrophys., Inst. für Extraterr. Phys., Garching, Federal Republic of Germany, 1973.

7. Haerendel, G., "Investigation of the Equatorial F-Region with Barium Clouds--a Review," presented at the 6th International Symposium on Equatorial Aeronomy, Aguadilla, July 1980.

8. Hanson, W. B., and S. Sanatani, "Large N_i Gradients Below the Equatorial-F Peak," J. Geophys. Res., 78, 1167, 1973.

9. Heelis, R. A., P. C. Kendall, R. J. Moffett, D. W. Windle, and H. Rishbeth, "Electrical Coupling of the E- and F-Regions and its Effects on F-Region Drifts and Winds," Planet. Space Sci., 22, 743, 1974.

10. Huba, J. D., P. K. Chaturvedi, S. L. Ossakow, and D. M. Towle, "High-Frequency Drift Waves with Wavelengths below the Ion Gyroradius in Equatorial Spread F," Geophys. Res. Lett., 5, 695, 1978.

11. Huba, J. D., and S. L. Ossakow, "On the Generation of 3-m Irregularities during Equatorial Spread F by Low-Frequency Drift Waves," J. Geophys. Res., 84, 6697, 1979.

12. Huba, J. D., and S. L. Ossakow, "On 11-cm Irregularities during Equatorial Spread F," J. Geophys. Res., accepted for publication, 1981.

13. Kelley, M. C., and E. Ott, "Two-Dimensional Turbulence in Equatorial Spread F," J. Geophys. Res., 83, 4369, 1978.

14. Kudeki, E., D. T. Farley, B. G. Fejer, and H. M. Ierkic, "Interfreometer Studies of Equatorial F-Region Irregularities and Drifts," submitted to Geophys. Res. Lett., 1981.

15. Linson, L. M., and J. B. Workman, "Formation of Striations in Ionospheric Plasma Clouds," J. Geophys. Res., 75, 3211, 1970.

16. Ossakow, J. L., and P. K. Chaturvedi, "Morphological Studies of Rising Equatorial Spread F Bubbles," J. Geophys. Res., 83, 2085, 1978.

17. Ossakow, S. L., S. T. Zalesak, B. E. McDonald, and P. K. Chaturvedi, "Nonlinear Spread F: Dependence on Altitude of the F Peak and Bottomside Background Electron Density Gradient Scale Length," J. Geophys. Res., 84, 17, 1979.

18. Rino, C. L., R. C. Livingston, B. C. Fair, and M. D. Cousins, "Continued Performance of the Wideband Satellite Experiment," Final Report, Contract DNA001-77-C-0220, SRI Project 6434, SRI International, Menlo Park, CA, June 1980.

19. Rino, C. L., R. T. Tsunoda, W. G. Chesnut, and D. R. McDaniel, "An Equatorial Experimental Program--Update," 12 January 1981, Concept Paper, SRI International, Menlo Park, CA.

20. Rishbeth, H., "Dynamics of the Equatorial F-Region," J. Atmos. Terr. Phys., 39, 1159, 1977.

21. Rishbeth, H., "Polarization Fields Produced by Winds in the Equatorial F-Region," Planet. Space Sci., 19, 357, 1971.

22. Scannapieco, A. J., and S. L. Ossakow, "Nonlinear Equatorial Spread F," Geophys. Res. Lett., 3, 451, 1976.

23. Sipler, D. P., and M. A. Biondi, "Equatorial F-Region Neutral Winds from Nightglow OI 630.00 nm Doppler Shifts," Geophys. Res. Lett., 5, 373, 1978.

24. Sperling, J. L., and S. R. Goldman, "Electron Collisional Effects on Lower Hybrid Drift Instabilities in the Ionosphere," J. Geophys. Res., 85, 3494, 1980.

25. Towle, D. M., "VHF and UHF Radar Observations of Equatorial F-Region Ionospheric Irregularities and Background Densities," Radio Sci., 15, 71, 1980.

26. Woodman, R. F., "Vertical Drift Velocities and East-West Electric Fields at the Magnetic Equator," J. Geophys. Res., 75, 6249, 1970.

27. Woodman, R. F., "East-West Ionospheric Drifts at the Magnetic Equator," Space Res. XII, 12, 969, 1972.

28. Woodman, R. F., and S. Basu, "Comparison between In-situ Spectral Measurements of F-Region Irregularities and Backscatter Observations at 3 m Wavelength," Geophys. Res. Lett., 5, 869, 1978.

29. Woodman, R. F., and C. Lattoz, "Radar Observations of F-Region Equatorial Irregularities," J. Geophys. Res., 81, 5447, 1976.

30. Workman, J. B., "The Relevance of Barium Releases to Problems of the Nuclear Environment," Topical Report, DNA 4514T, Contract DNA001-76-C-0136, Berkeley Research Associates, Inc., Berkeley, CA, December 1977.

31. Zalesak, S. T., and S. L. Ossakow, "Nonlinear Equatorial Spread F: Spatially Large Bubbles Resulting from Large Horizontal Scale Initial Perturbations," J. Geophys. Res., 85, 2131, 1980.

32. Zalesak, S. T., S. L. Ossakow, and P. K. Chaturvedi, "An Explanation of Westward Tilts, "Fishtails," and "Cs" in the Equatorial Spread F Ionosphere," presented at the Fall AGU Meeting, San Francisco, CA, 1980.

Appendix

PUBLICATIONS RELATING TO THE ALTAIR PROJECT

1. Tsunoda, R. T., M. J. Baron, and J. Owen, "ALTAIR: An Incoherent Scatter Radar for Equatorial Spread F Studies," DNA 4538T, Contract DNA001-77-C-0220, SRI International, Menlo Park, CA, January 1978.

2. Tsunoda, R. T., M. J. Baron, J. Owen, and D. M. Towle, "ALTAIR: An Incoherent Scatter Radar for Equatorial Spread F Studies," Radio Sci., 14, 1111, 1979.

3. Tsunoda, R. T., "On the Spatial Relationship of 1-Meter Equatorial Irregularities and Depletions in Total Electron Content," DNA 4897T, Topical Report 1, Contract DNA001-79-C-0153, SRI International, Menlo Park, CA, 1 February 1979.

4. Tsunoda, R. T., and D. M. Towle, "On the Spatial Relationship of 1-Meter Equatorial Spread-F Irregularities and Depletions in Total Electron Content," Geophys. Res. Lett., 6, 873, 1979.

5. Tsunoda, R. T., "On the Spatial Relationship of 1-Meter Equatorial Spread-F Irregularities and Plasma Bubbles," DNA 4935T, Topical Report 2, Contract DNA001-79-C-0153, SRI International, Menlo Park, CA, 1 April 1979; and J. Geophys. Res., 85, 185, 1980.

6. Tsunoda, R. T., "Magnetic-Field-Aligned Characteristics of Plasma Bubbles in the Nighttime Equatorial Ionosphere," DNA 5150T, Topical Report 3, Contract DNA001-79-C-0153, SRI International, Menlo Park, CA, 1 July 1979; and J. Atmos. Terr. Phys., 42, 743, 1980.

7. Tsunoda, R. T., "The Growth and Decay of Equatorial Backscatter Plumes," DNA 5249T, Topical Report 4, Contract DNA001-79-C-0153, SRI International, Menlo Park, CA, 1 February 1980.

8. Tsunoda, R. T., "Backscatter Measurements of 11-cm Equatorial Spread-F Irregularities," DNA 5324T, Topical Report 5, Contract DNA001-79-C-0153, SRI International, Menlo Park, CA, 1 June 1980; and Geophys. Res. Lett., 7, 848, 1980.

9. Szuszczewicz, E. P., R. T. Tsunoda, R. Narcisi, and J. C. Holmes, "Coincident Radar and Rocket Observations of Equatorial Spread F," Geophys. Res. Lett., 7, 537, 1980.

10. Tsunoda, R. T., "Time Evolution and Dynamics of Equatorial Backscatter Plumes--1. Growth Phase," J. Geophys. Res., 86, 139, 1981.

11. Tsunoda, R. T., and B. R. White, "On the Generation and Growth of Equatorial Backscatter Plumes--1. Wave Structure in the Bottomside F Layer," J. Geophys. Res., accepted for publication, 1981; and in Proc. Summer Equatorial Experiment Data Review Meeting, 18 March 1980, compiled by D. R. McDaniel, Contract DNA001-78-C-0379, SRI International, Menlo Park, CA, p. 227, November 1980.

12. Rino, C. L., R. T. Tsunoda, J. Petriceks, R. C. Livingston, M. C. Kelley, and K. D. Baker, "Simultaneous Rocketborne Beacon and In-situ Measurements of Equatorial Spread F," J. Geophys. Res., accepted for publication, 1981.

13. Kelley, M. C., R. Pfaff, K. D. Baker, J. C. Ulwick, R. Livingston, C. Rino, and R. Tsunoda, "Simultaneous Rocket Probe and Radar Measurements of Equatorial Spread F--Transitional and Short Wavelength Results," J. Geophys. Res., submitted 1981.

14. Tsunoda, R. T., "ALTAIR Radar Measurements in Support of the PLUMEX Rocket Campaign," in Proc. Summer Equatorial Experiment Data Review Meeting, 18 March 1980, compiled by D. R. McDaniel, Contract DNA001-78-C-0379, SRI International, Menlo Park, CA, p. 51, November 1980.

15. Szuszczewicz, E. P., R. Tsunoda, R. Narcisi, and J. Holmes, "PLUMEX II--A Second Set of Coincident Radar and Rocket Observations of Equatorial Spread F," in Proc. Summer Equatorial Experiment Data Review Meeting, 18 March 1980, compiled by D. R. McDaniel, Contract DNA001-78-C-0379, SRI International, Menlo Park, CA, p. 195, November 1980; and Geophys. Res. Lett., submitted 1981.

16. Tsunoda, R. T., R. C. Livingston, and C. L. Rino, "Evidence of a Velocity Shear in Bulk Plasma Motion Associated with the Post-Sunset Rise of the Equatorial F Layer," this report (Section III-E); and Geophys. Res. Lett., accepted for publication, 1981.

DISTRIBUTION LIST

DEPARTMENT OF DEFENSE

Assistant Secretary of Defense
Comm, Cmd, Cont & Intell
ATTN: Dir of Intelligence Sys, J. Babcock

Assistant to the Secretary of Defense
Atomic Energy
ATTN: Executive Assistant

Command & Control Technical Center
ATTN: C-312, R. Mason
ATTN: C-650, G. Jones
3 cy ATTN: C-650, W. Heidig

Defense Communications Agency
ATTN: Code 480
ATTN: Code 480, F. Dieter
ATTN: Code 810, J. Barna
ATTN: Code 205
ATTN: Code 101B

Defense Communications Engineer Center
ATTN: Code R123
ATTN: Code R410, N. Jones

Defense Intelligence Agency
ATTN: DT-5
ATTN: DB-4C, E. O'Farrell
ATTN: DB, A. Wise
ATTN: DT-1B
ATTN: Dir, E. Tighe
ATTN: DC-7D, W. Wittig

Defense Nuclear Agency
ATTN: NAFD
ATTN: STNA
ATTN: RAEE
ATTN: NATD
3 cy ATTN: RAAE
4 cy ATTN: TITL

Defense Technical Information Center
12 cy ATTN: DD

Field Command
Defense Nuclear Agency
ATTN: FCPR

Field Command
Defense Nuclear Agency
Livermore Branch
ATTN: FCPRL

Interservice Nuclear Weapons School
ATTN: TTV

Joint Chiefs of Staff
ATTN: C3S
ATTN: C3S, Evaluation Office

Joint Strategic Tgt Planning Staff
ATTN: JLTW-2
ATTN: JLA

National Security Agency
ATTN: W-32, O. Bartlett
ATTN: B-3, F. Leonard
ATTN: R-52, J. Skillman

DEPARTMENT OF DEFENSE (Continued)

Under Secretary of Defense for Rsch & Engrg
ATTN: Strategic & Space Sys (OS)

WWMCCS System Engineering Org
ATTN: R. Crawford

DEPARTMENT OF THE ARMY

Assistant Chief of STaff for Automation & Comm
Department of the Army
ATTN: DAAC-ZT, P. Kenny

Atmospheric Sciences Laboratory
U.S. Army Electronics R & D Command
ATTN: DELAS-EO, F. Niles

BMD Advanced Technology Center
Department of the Army
ATTN: ATC-T, M. Capps
ATTN: ATC-O, W. Davies

BMD Systems Command
Department of the Army
2 cy ATTN: BMDSC-HW

Deputy Chief of Staff for Ops & Plans
Department of the Army
ATTN: DAMO-RQC

Harry Diamond Laboratories
Department of the Army
ATTN: DELHD-I-TL, M. Weiner
ATTN: DELHD-N-P, F. Wimenitz
ATTN: DELHD-N-RB, R. Williams
ATTN: DELHD-N-P

U.S. Army Chemical School
ATTN: ATZN-CM-CS

U.S. Army Comm-Elec Engrg Instal Agency
ATTN: CCC-EMEO-PED, G. Lane
ATTN: CCC-CED-CCO, W. Neuendorf

U.S. Army Communications Command
ATTN: CC-OPS-W
ATTN: CC-OPS-WR, H. Wilson

U.S. Army Communications R&D Command
ATTN: DRDCO-COM-RY, W. Kesselman

U.S. Army Foreign Science & Tech Ctr
ATTN: DRXST-SD

U.S. Army Materiel Dev & Readiness Cmd
ATTN: DRCLDC, J. Bender

U.S. Army Missile Intelligence Agency
ATTN: J. Gamble

U.S. Army Nuclear & Chemical Agency
ATTN: Library

U.S. Army Satellite Comm Agency
ATTN: Document Control

DEPARTMENT OF THE ARMY (Continued)

U.S. Army TRADOC System Analysis Activity
ATTN: ATAA-PL
ATTN: ATAA-TDC
ATTN: ATAA-TCC, F. Payan, Jr.

DEPARTMENT OF THE NAVY

Joint Cruise Missiles Project Office
Department of the Navy
ATTN: JCMG-707

Naval Air Development Center
ATTN: Code 6091, M. Setz

Naval Air Systems Command
ATTN: PMA 271

Naval Electronic Systems Command
ATTN: PME 106-4, S. Kearney
ATTN: PME-117-2013, G. Burnhart
ATTN: PME 117-20
ATTN: Code 3101, T. Hughes
ATTN: Code 501A
ATTN: PME 106-13, T. Griffin
ATTN: PME 117-211, B. Kruger

Naval Intelligence Support Center
ATTN: NISC-50

Naval Ocean Systems Center
ATTN: Code 532, J. Bickel
ATTN: Code 5322, M. Paulson
3 cy ATTN: Code 5323, J. Ferguson
3 cy ATTN: Code 5324, W. Moler

Naval Research Laboratory
ATTN: Code 7550, J. Davis
ATTN: Code 4187
ATTN: Code 4780, S. Ossakow
ATTN: Code 7500, B. Wald
ATTN: Code 7950, J. Goodman
ATTN: Code 1700, T. Coffey

Naval Space Surveillance System
ATTN: J. Burton

Naval Surface Weapons Center
ATTN: Code F31

Naval Telecommunications Command
ATTN: Code 341

Office of Naval Research
ATTN: Code 465
ATTN: Code 420
ATTN: Code 421

Office of the Chief of Naval Operations
ATTN: OP 65
ATTN: OP 941D
ATTN: OP 981N

Strategic Systems Project Office
Department of the Navy
ATTN: NSP-2722, F. Wimberly
ATTN: NSP-2141
ATTN: NSP-43

DEPARTMENT OF THE AIR FORCE

Aerospace Defense Command
Department of the Air Force
ATTN: DC, T. Long

Air Force Geophysics Laboratory
ATTN: OPR, H. Gardiner
ATTN: OPR-1
ATTN: LKB, K. Champion
ATTN: OPR, A. STair
ATTN: S. Basu
ATTN: PHP
ATTN: PHI, J. Buchau
ATTN: R. Thompson

Air Force Weapons Laboratory
Air Force Systems Command
ATTN: SUL
ATTN: NTYC
ATTN: NTN

Air Force Wright Aeronautical Lab
ATTN: W. Hunt
ATTN: A. Johnson

Air Logistics Command
Department of the Air Force
ATTN: OO-ALC/MM, R. Blackburn

Air University Library
Department of the Air Force
ATTN: AUL-LSE

Air Weather Service, MAC
Department of the Air Force
ATTN: DNXP, R. Babcock

Assistant Chief of Staff
Intelligence
Department of the Air Force
ATTN: INED

Assistant Chief of Staff
Studies & Analyses
Department of the Air Force
ATTN: AF/SASC, W. Keaus
ATTN: AF/SASC, C. Rightmeyer

Ballistic Missile Office
Air Force Systems Command
ATTN: MNNXH, J. Allen

Deputy Chief of Staff
Operations, Plans, and Readiness
Department of the Air Force
ATTN: AFXOKT
ATTN: AFXOKS
ATTN: AFXOXFD
ATTN: AFXOKCD

Deputy Chief of Staff
Research, Development, & Acq
Department of the Air Force
ATTN: AFRDS
ATTN: AFRDSS
ATTN: AFRDSP

DEPARTMENT OF THE AIR FORCE (Continued)

Electronic Systems Division
ATTN: DCKC, J. Clark

Electronic Systems Division
ATTN: XRW, J. Deas

Electronic Systems Division
ATTN: YSM, J. Kobelski
ATTN: YSEA

Foreign Technology Division
Air Force Systems Command
ATTN: TQTD, B. Ballard
ATTN: NIIS Library

Headquarters Space Division
Air Force Systems Command
ATTN: SKY, C. Kennedy
ATTN: SKA, D. Bolin

Headquarters Space Division
Air Force Systems Command
ATTN: YZJ, W. Mercer

Headquarters Space Division
Air Force Systems Command
ATTN: E. Butt

Rome Air Development Center
Air Force Systems Command
ATTN: OCS, V. Coyne
ATTN: TSLD

Rome Air Development Center
Air Force Systems Command
ATTN: EEP

Strategic Air Command
Department of the Air Force
ATTN: DCXT
ATTN: NRT
ATTN: DCXR, T. Jorgensen
ATTN: DCX
ATTN: XPFS

OTHER GOVERNMENT AGENCIES

Central Intelligence Agency
ATTN: OSWR/NED

Department of Commerce
National Bureau of Standards
ATTN: Sec Ofc for R. Moore

Department of Commerce
National Oceanic & Atmospheric Admin
ATTN: R. Grubb

Institute for Telecommunications Sciences
ATTN: A. Jean
ATTN: L. Berry
ATTN: W. Utlaut

U.S. Coast Guard
Department of Transportation
ATTN: G-DOE-3/TP54, B. Romine

DEPARTMENT OF ENERGY CONTRACTORS

EG&G, Inc
Los Alamos Division
ATTN: J. Colvin
ATTN: D. Wright

Lawrence-Livermore National Lab
ATTN: L-389, R. Ott
ATTN: L-31, R. Hager
ATTN: Technical Info Dept Library

Los Alamos National Scientific Lab
ATTN: MS 664, J. Zinn
ATTN: D. Simons
ATTN: P. Keaton
ATTN: D. Westervelt
ATTN: E. Jones
ATTN: R. Taschek
ATTN: MS 670, J. Hopkins

Sandia National Laboratories
Livermore Laboratory
ATTN: B. Murphey
ATTN: T. Cook

Sandia National Lab
ATTN: ORG 1250, W. Brown
ATTN: ORG 4241, T. Wright
ATTN: Space Project Div
ATTN: 3141
ATTN: D. Thornbrough
ATTN: D. Dahlgren

DEPARTMENT OF DEFENSE CONTRACTORS

Aerospace Corp
ATTN: I. Garfunkel
ATTN: S. Bower
ATTN: D. Olsen
ATTN: N. Stockwell
ATTN: R. Slaughter
ATTN: V. Josephson
ATTN: T. Salmi
ATTN: J. Straus

University of Alaska
ATTN: T. Davis
ATTN: N. Brown
ATTN: Tech Library

Aanlytical Systems Engineering Corp
ATTN: Radio Sciences

Analytical Systems Engineering Corp
ATTN: Security

Barry Research Corporation
ATTN: J. McLaughlin

BDM Corp
ATTN: T. Neighbors
ATTN: L. Jacobs

Berkeley Research Associates, Inc
ATTN: J. Workman

Betac
ATTN: J. Hirsch

DEPARTMENT OF DEFENSE CONTRACTORS (Continued)

Boeing Co
ATTN: M/S 42-33, J. Kennedy
ATTN: G. Hall
ATTN: S. Tashird

Booz-Allen & Hamilton, Inc
ATTN: B. Wilkinson

University of California at San Diego
ATTN: H. Booker

Charles Stark Draper Lab, Inc
ATTN: J. Gilmore
ATTN: D. Cox

Communications Satellite Corp
ATTN: D. Fang

Comsat Labs
ATTN: G. Hyde
ATTN: R. Taur

Cornell University
ATTN: M. Kelly
ATTN: D. Farley, Jr

Electrospace Systems, Inc
ATTN: H. Logston

ESL, Inc
ATTN: J. Marshall

General Electric Co
Space Division
ATTN: M. Bortner
ATTN: A. Harcar

General Electric Co
Re-Entry Systems Division
ATTN: A. Steinmayer
ATTN: C. Zierdt

General Electric Co
ATTN: F. Reibert

General Electric Tech Services Co., Inc
ATTN: G. Millman

General Research Corp
Santa Barbara Division
ATTN: J. Ise, Jr
ATTN: J. Garbarino

Horizons Technology, Inc
ATTN: R. Kruger

HSS, Inc
ATTN: D. Hansen

IBM Corp
Federal Systems Divison
ATTN: F. Ricci

University of Illinois
ATTN: Security Supervisor for K. Yeh

VisiDyne, Inc
ATTN: C. Humphrey
ATTN: J. Carpenter

DEPARTMENT OF DEFENSE CONTRACTORS (Continued)

Institute for Defense Analyses
ATTN: J. Bengston
ATTN: E. Bauer
ATTN: H. Wolfhard
ATTN: J. Aein

International Tel & Telegraph Corp
ATTN: G. Wetmore
ATTN: Tech Library

JAYCOR
ATTN: J. Sperling

JAYCOR
ATTN: J. Doncarlos

Johns Hopkins University
ATTN: T. Potemra
ATTN: J. Phillips
ATTN: T. Evans
ATTN: J. Newland
ATTN: P. Komiske

Kaman Tempo
ATTN: DASIAC
ATTN: W. McNamara
ATTN: T. Stephens
ATTN: W. Knapp

Linkabit Corp
ATTN: I. Jacobs

Litton Systems, Inc
Amecom Division
ATTN: R. Grasty

Lockheed Missiles & Space Co, Inc
ATTN: W. Imhof
ATTN: M. Walt
ATTN: R. Johnson

Lockheed Missiles & Space Co, Inc
ATTN: Dept 60-12

M.I.T. Lincoln Lab
ATTN: D. Towle

Martin Marietta Corp
ATTN: R. Heffner

McDonnell Douglas Corp
ATTN: J. Moule
ATTN: R. Halprin
ATTN: W. Olson
ATTN: G. Mroz
ATTN: N. Harris

Meteor Communications Consultants
ATTN: R. Leader

Mission Research Corp
ATTN: S. Gutsche
ATTN: R. Hendrick
ATTN: D. Sappenfield
ATTN: F. Fajen
ATTN: R. Bogusch
ATTN: R. Kilb
ATTN: Tech Library

DEPARTMENT OF DEFENSE CONTRACTORS (Continued)

Mitre Corp
ATTN: G. Harding
ATTN: A. Kymmel
ATTN: B. Adams
ATTN: C. Callahan

Mitre Corp
ATTN: M. Horrocks
ATTN: J. Wheeler
ATTN: W. Foster
ATTN: W. Hall

Pacific-Sierra Research Corp
ATTN: E. Field, Jr
ATTN: F. Thomas
ATTN: H. Brode

Pennsylvania State University
ATTN: Ionospheric Research Lab

Photometrics, Inc
ATTN: I. Kofsky

Physical Dynamics, Inc
ATTN: E. Fremouw

Physical Research, Inc
ATTN: R. Deliberis

R & D Associates
ATTN: R. Turco
ATTN: F. Gilmore
ATTN: B. Gabbard
ATTN: M. Gantsweg
ATTN: C. Greifinger
ATTN: W. Wright
ATTN: R. Lelevier
ATTN: W. Karzas
ATTN: H. Ory
ATTN: P. Haas

R & D Associates
ATTN: B. Yoon

Rand Corp
ATTN: C. Crain
ATTN: E. Bedrozian

Riverside Research Institute
ATTN: V. Trapani

Rockwell International Corp
ATTN: R. Buckner

DEPARTMENT OF DEFENSE CONTRACTORS (Continued)

Rockwell International Corp
ATTN: S. Quilici

Santa Fe Corp
ATTN: D. Paolucci

Science Applications, Inc
ATTN: E. Straker
ATTN: D. Hamlin
ATTN: L. Linson
ATTN: C. Smith

Science Applications, Inc
ATTN: SZ

Science Applications, Inc
ATTN: J. Cockayne

SRI International
ATTN: W. Jaye
ATTN: R. Leadabrand
ATTN: D. Neilson
ATTN: C. Rino
ATTN: J. Petrickes
ATTN: W. Chesnut
ATTN: R. Livingston
4 cy ATTN: R. Tsunoda
ATTN: G. Smith
ATTN: G. Price
ATTN: M. Baron
ATTN: A. Burns

Sylvania Systems Group
ATTN: M. Cross

Technology International Corp
ATTN: W. Boquist

TRI-COM, Inc
ATTN: D. Murray

TRW Defense & Space Sys Group
ATTN: D. Dee
ATTN: R. Plebuch

Utah State University
ATTN: L. Jensen
ATTN: K. Baker
ATTN: J. Dupnik